specificity protein kinases, members of the MAPK kinase family. In contrast, in the absence of a signal the constituents of the MAPK cascade return to their inactive dephosphorylated state, suggesting an essential role for protein phosphatases in the negative regulation of the MAPK cascade. Protein phosphatases are classified into three groups, protein serine/threonine phosphatases, protein tyrosine phosphatases (PTPs) and protein dual specificity serine/threonine/tyrosine phosphatases (DSPs), depending on their phosphoamino acid specificity [6].

Dehydroepiandrosterone-sulfate (DHEA-S), the sulfated form of DHEA, is the most abundant steroids in young adults, but gradually decline with aging. Although the molecular basis of DHEA action still remains to be elucidated, recent findings have suggested modulatory actions of DHEA on the MAPK signal transduction pathway [7–9]. To date, much data have been accumulated on the biological action of DHEA, although some of these were carried out using rodents in which the P450 C17 activities are extremely low, thus leading to trace or nearly undetectable levels of serum DHEA or DHEAS concentrations. In humans, the clinical application of DHEA targeting hormone replacement therapy [10–13] has been tested in clinical trials.

We have been interested in the actions of DHEA using both in vitro and in vivo experiments [14] (for review). We have previously reported that a human clonal T lymphocyte, the PEER cell [15], which is stimulated with phorbol-12-myristate-13-acetate (PMA) and calcium ionophore A23187 to mimic the activation of the T-cell antigen receptor (TcR), revealed the specific binding of [3H]-DHEA to its putative receptor. This specific binding was further increased when treated with 100 nM of DHEA itself in addition to the PMA and A23187 treatment [16], while the subcellular localization of the DHEA-bound molecule(s) was not determined. In the experiment, the MAPK cascade was activated by PMA, which bypasses all receptor-induced proximal tyrosine phosphorylation events by directly activating the Raf kinase through protein kinase C [17,18]. Thus, PEER cells are likely to provide a good model for investigating the cellular phenotypes altered by the DHEA action on the MAPK cascade, or for identifying the putative receptor for DHEA. Here, we report that DHEA negatively regulates the MAPK pathway in humans via a novel MAPK phosphatase, tentatively named DDSP (DHEA-enhanced DSP), which is highly homologous to LCPTP/HePTP [19,20] not only controlling the activity of MAPKs but also mediating crosstalk between the cAMP system and the MAPK cascade [21].

2. Materials and methods

2.1. Cells

Human T lymphoblastic leukemic cells, PEER, were maintained in RPMI 1640 (Gibco) supplemented with 10% FBS, 60 μg/ml of benzylpenicillin, 100 μg/ml of streptomycin, 2 mmol/L of L-glutamine, and 50 μmol/L of 2-mercaptoethanol. The cells were plated at a concentration of 1×10^5/ml and then treated with 5 nM PMA and 500 ng/ml of calcium ionophore A23187 in the presence or absence of 50 to 100 nM of DHEA (PEER(+) and PEER(−), respectively) for 28 h. NIH3T3 mouse fibroblasts were maintained in DMEM (Gibco) supplemented with 10% FBS, 60 μg/ml of benzylpenicillin, 100 μg/ml of streptomycin, and 2 mmol/L of L-glutamine.

2.2. Suppression subtractive hybridization screening and reverse transcribed-PCR (RT-PCR)

Total RNA was isolated using ISOGEN (Nippon Gene Co.). Suppression subtraction hybridization (SSH) was performed to construct a subtraction cDNA library using a commercially available kit (PCR-Select cDNA Subtraction Kit, Clonetech Laboratories Inc.). Briefly, double-stranded cDNAs were synthesized using the poly(A)$^+$RNAs from PEER(+) or PEER(−) cells. After the completion of two rounds of hybridization, the suppression PCR products were amplified using the GeneAmp 9600 PCR System (Perkin Elmer Applied Biosystems Division), size-fractionated using Chroma Spin+TE-200 Columns (Clontech Laboratories Inc.) and then blunt ligated into pBluescript II SK—which was cleaved with *Sma*I. DH5α was transformed with the ligation mixtures to construct the plasmid library without amplification.

The nucleotide sequences of 400 randomly chosen clones were determined using a DSQ-1000 DNA Sequencer (Shimadzu Co) and subjected to a homology search. PCR primers of 16-mers specific for the nucleotide sequence of each clone were synthesized and used for RT-PCR to confirm the effect of the DHEA treatment. Semiquantitative RT-PCR was performed using total RNAs from untreated PEER cells, PEER(+) and PEER(−) cells. The PCR fragments were electrophoresed in a 4% polyacrylamide gel. The gels were stained with Cyber Green (Amersham Life Science) and the intensities of the fluorescent signals were analyzed directly using a STORM 860 Image Analyzer (Molecular Dynamics Inc.). A phage cDNA library using the mRNAs from PEER (+) cells was constructed using a ZAP-cDNA Synthesis Kit (Stratagene) and then probed with a clone 1–20 cDNA insert. Thereafter, 1×10^6 plaques were subjected to screening.

2.3. Phosphatase assay

The full-length cDNA sequence of DDSP was ligated into the pAcGHLT baculovirus expression vector (Pharmingen), containing a 6× histidine tag and a glutathione *S*-transferase (GST) tag upstream of the multiple cloning sites, and then transfected into SF-9 (*Spodoptera frugiperda* pupal ovary) insect cells using the calcium phosphate precipitation method. Cells were grown at 25 °C and the viruses were enriched according to the manufacturer's protocol. The expressed GST-DDSP protein was purified using a glutathione sepharose affinity column. Phosphatase assays were performed using the Tyrosine Phosphatase Assay System and the Serine/Threonine Phosphatase Assay System (Promega Co.).

2.4. Tissue distribution and hormonal regulation of DDSP mRNA

The tissue distribution and hormonal regulation of DDSP or LCPTP/HePTP mRNA were examined by semiquantitative RT-

PCR. To compare the tissue distribution and steroid hormone-specific mRNA induction between DDSP and LCPTP/HePTP, 2 sets of primers were designed (Fig. 1), namely one for amplifying the sequences specific to DDSP (5′-GGA-TATTGTGTGCCAACTGC-3′ for the forward and 5′-GAGA-CAGGGTTTACACCATG-3′ for the reverse) and the other for amplifying the sequences specific to LCPTP/HePTP (5′-CAGCTGCTTCAGCAGACCTC-3′ for the forward and 5′-

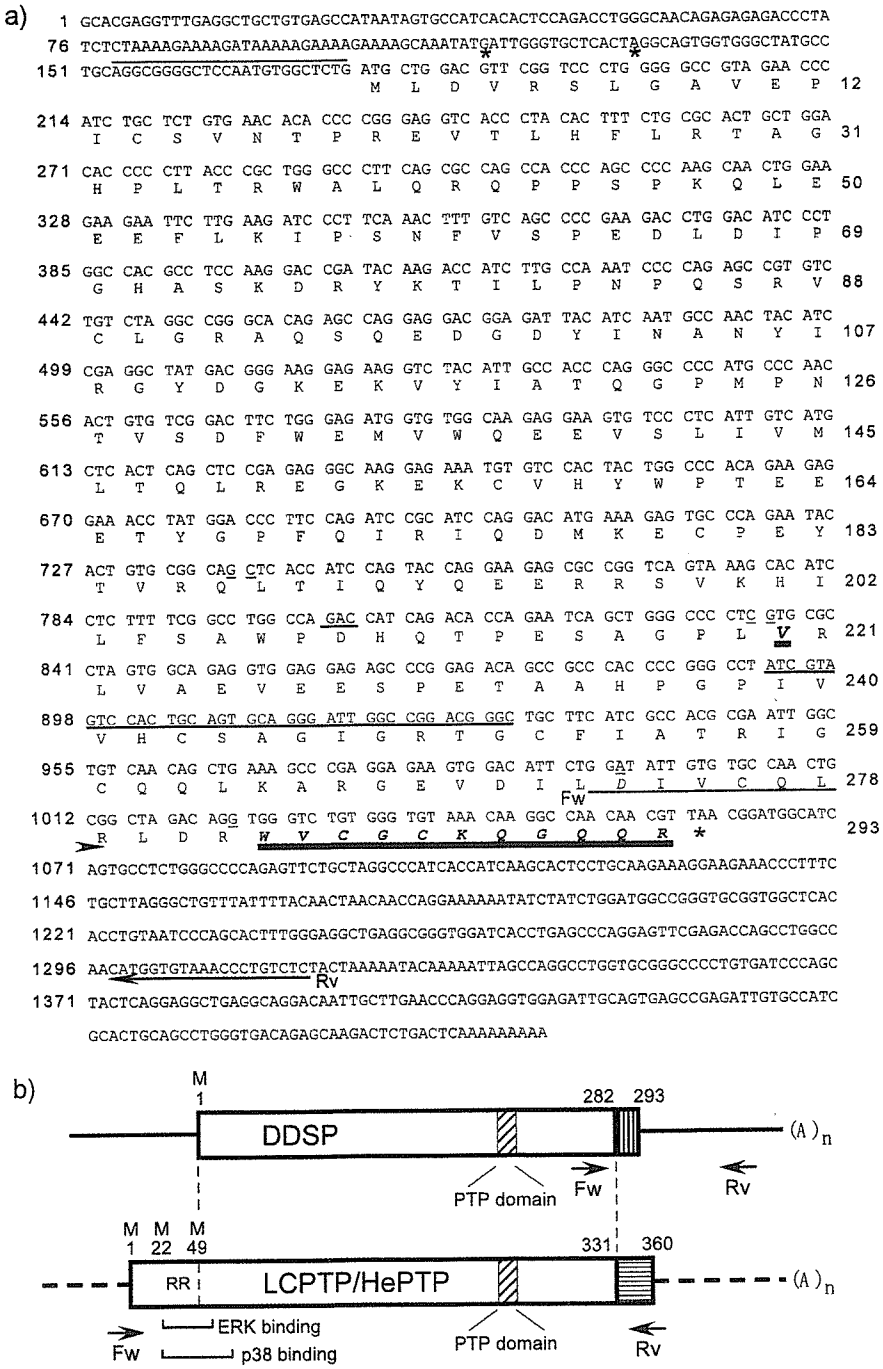

Fig. 1. The structure of DDSP. (a) The nucleotide and aa sequence of DDSP. The nucleotide number and the aa residue number are shown on the left side and right side, respectively. The substitution of the LCPTP/HePTP amino acid residues with the DDSP specific residues are highlighted by italic letters and bold lines, and the 2 termination codons are shown by asterisks. The putative PTP/DSP catalytic domain and Asp209, which is thought to be critical for PTP/DSP activity, are underlined. Arrows labeled with Fw and Rv are forward (Fw) and reverse (Rv) primers, respectively. (b) Schematic comparison of the DDSP structure with the LCPTP/HePTP structure. In DDSP, the aa residues required for ERK binding (including Arg41 and Arg42 shown as "RR" in the figure) are lacking (see text). The C-terminal 11 aa residues of DDSP (vertical bars) are different from those of LCPTP/HePTP (horizontal bars). The dashed box represents the PTP/DSP central catalytic domain. Arrows labeled with Fw and Rv are forward (Fw) and reverse (Rv) primers, respectively.

GGGGCTGGGTTCCTCAGGCA-3′ for the reverse). Tissue cDNA panels (Clontech Laboratories Inc.) were used for the RT-PCR.

2.5. Subcellular localization of DDSP

The full length DDSP cDNA sequence was ligated in-frame into pEGFP (Clontech), thus generating pDDSP-GFP in which the C′-terminus of the DDSP sequence was fused to the N′-terminus of green fluorescence protein (GFP). pDDSP-GFP was transfected into COS-7 cells and the cells were observed using a Leica TCS-SP System confocal laser microscope (Leica Microsystems). The cells were imaged for green fluorescence by excitation with the 488 nm line from an argon laser and the emission was viewed through a 496 to 505 nm band pass filter.

2.6. Immunocoprecipitation and Western blot analysis

For the immunocoprecipitation experiments, NIH3T3 mouse fibroblasts were transfected with a plasmid expressing flag-tagged DDSP using Superfect (Qiagen). At 24 h posttransfection, the cells were stimulated with 0.5 M NaCl for 20 min (for p38- and JNK-MAPK) or 50 ng/ml of PMA for 15 min after incubation in a serum free medium for 15 h (for ERK). Whole cell lysates were prepared by lysing the cells in a buffer (1.0% Nonidet P-40, 50 mM Tris–HCl pH 7.8, 150 mM NaCl, 1 mM DTT, 1 tablet of a protease inhibitor cocktail (Roche)). The lysates were incubated at 4 °C for 1 h with antibodies against ERK, JNK- or p38-MAPK (Cell Signaling) in an immunoprecipitation buffer (0.5% Nonidet P-40, 1 mM EDTA, 50 mM Tris–HCl pH 7.8, 200 mM NaCl, 1 mM DTT, 1 tablet of the protease inhibitor cocktail), and then further incubated with protein-A sepharose beads (Pharmacia) at 4 °C for 2 h. For Western blotting, the samples were separated by SDS-PAGE, transferred to a nitrocellulose filter, and then probed with an antibody against flag according to the manufacturer's protocol. To test the inactivation of the MAPK pathway by DDSP, two sets of transfection experiments were performed. In one experiment, the flag-tagged DDSP cDNA was transfected into NIH3T3 cells, and the transfected cells were then treated to activate ERK, p38 or JNK-MAPKs as in the immunocoprecipitation experiments. The transfection efficiency was monitored by the transfection of pEGFP in a separate dish and resulted in 30 to 50% efficiency. Western blotting was performed to observe the dephosphorylation of endogenous MAPK in the whole cell lysates of transfected cells using anti-phospho-MAPK antibodies (Cell Signaling). To observe the dephosphorylation of the endogenous activated MAPKs, the MACSelect system (Miltenyi Biotech) was used to enrich the transfected cells. The flag-tagged DDSP cDNA was ligated into the pMACSK^{k}II vector plasmid to generate pMACS-DDSP and the NIH3T3 cells were transfected in a 10 cm dish with 20 μg of pMACS-DDSP, or pMACSK^{k}II as a control. The transfected cells were subjected to affinity-column separation and then treated with 0.4 M sorbitol for 20 min to activate p38-MAPK, or 50 ng/ml of PMA for 15 min after incubation in a serum free medium for 20 h for ERK. Nearly 80% of the recovered cells were revealed to be transfected when the efficiency was preliminarily monitored by the cotransfection of pMACSK^{k}II and pEGFP. Western blotting was performed using anti-phospho-p38 or -ERK antibodies (Cell Signaling).

3. Results

3.1. Isolation of a cDNA sequence homologous to LCPTP/HePTP

Human T-cell leukemia cells (PEER) were treated with PMA and calcium ionophore A23187 to mimic TcR activation with (PEER(+)) or without (PEER(−)) 50 nM of DHEA. We performed the SSH screening by constructing a cDNA library in which the cDNAs from PEER(−) cells were subtracted from those from PEER(+) cells. After the SSH subtraction, the cDNAs for the MAPK phosphatases were enriched. One of these clones (named 1–20) contained 600 bases of sequence highly homologous to a leukocyte-specific PTP (LCPTP), also known as hematopoietic tissue-specific PTP (HePTP), a sequence which was originally isolated as a cytoplasmic PTP [19,20].

However, 1–20 contained another 150 bases of unique sequence and thus a phage cDNA library from the activated PEER cells was screened to obtain the full-length cDNA. The translation of the full length 1–20 (DDSP) cDNA sequence revealed one long open reading frame consisting of 293 amino acid (aa) residues, and also a striking homology (96% homology at the aa level) to LCPTP/HePTP (Fig. 1a). In the 50 aa residues of the LCPTP/HePTP N-terminus, there were 3 methionine (Met) residues: translation initiation Met 1 for LCPTP, translation initiation Met 22 for HePTP and Met 49 (Fig. 1b). A putative translation initiation Met for 1–20 corresponded to Met 49 of the LCPTP. And the preceding 24 nt of the 5′ noncoding sequence were identical to those of LCPTP/HePTP (sequence encoding aa residues 41 to 48 of LCPTP, as shown by the thin line above the nucleotide sequence preceding the translation initiation Met for 1–20 in Fig. 1a). However, about 150 bases of the sequence further upstream, including 2 in-frame termination codons, were unique. Although the aa sequence known as the PTP/DSP central catalytic domain was highly conserved, the striking homology to LCPTP/HePTP was disrupted at the C-terminal end, resulting in 11 novel aa sequences (Fig. 1a). Interestingly, the first 25 nt sequences encoding these 11 aa residues were identical to the partial sequence reported for the exon 9/intron 9 junction of LCPTP/HePTP [22].

A BLAST search of the human genome sequence using the 5′- and 3′-noncoding regions of 1–20 assigned each sequence to within the PTPN7 locus on chromosome 1q31 (the 5′-noncoding sequence was the intron 2/exon 3 junction, and the 3′-noncoding sequence was the read-through of the exon 9/intron 9 junction downstream to intron 9) that encodes LCPTP/HePTP, thus strongly suggesting that the 1–20 sequence was a novel alternatively spliced variant of the PTPN7 gene. Another RT-PCR experiment using RNA from human peripheral blood lymphocytes with or without reverse transcription confirmed that the full-length cDNA derived from the mRNA (data not shown).

3.2. *Phosphatase activity*

To test whether or not clone 1–20 possessed phosphatase activities, a GST fusion product with 1–20 was expressed in SF-9 insect cells since bacterially expressed fusion proteins always formed inclusion bodies. SDS-PAGE showed a stably expressed fusion protein with the expected molecular weight (data not shown). The expressed protein showed a rapid loss of phosphate from the phosphotyrosine in a time dependent manner. The activity was strongest at pH 6.0, and was suppressed by the PTP specific inhibitor sodium orthovanadate (Na_3VO_4) (Fig. 2a). In contrast to LCPTP/HePTP, the expressed 1–20 protein also caused a rapid loss of the phosphate from the phosphothreonine. Although threonine phosphatase activity was weaker (about 50% at the optimal pH 8.0) compared to tyrosine phosphatase activity at the optimal pH, the activity was suppressed by sodium fluoride (NaF), a serine/threonine phosphatase specific inhibitor (Fig. 2b).

3.3. *Subcellular localization*

The DDSP sequence was in-frame ligated into pEGFP generating pEGFP-DDSP which was transfected into COS-7 cells to observe the subcellular localization of GFP fluorescence. The GFP fluorescence was detected solely in the cytoplasm as in the case of LCPTP/HePTP. Furthermore, the distribution of the GFP-fluorescence was homogeneous, suggesting that this protein was not associated with the membrane structure (Fig. 3a). The treatment of the trans-

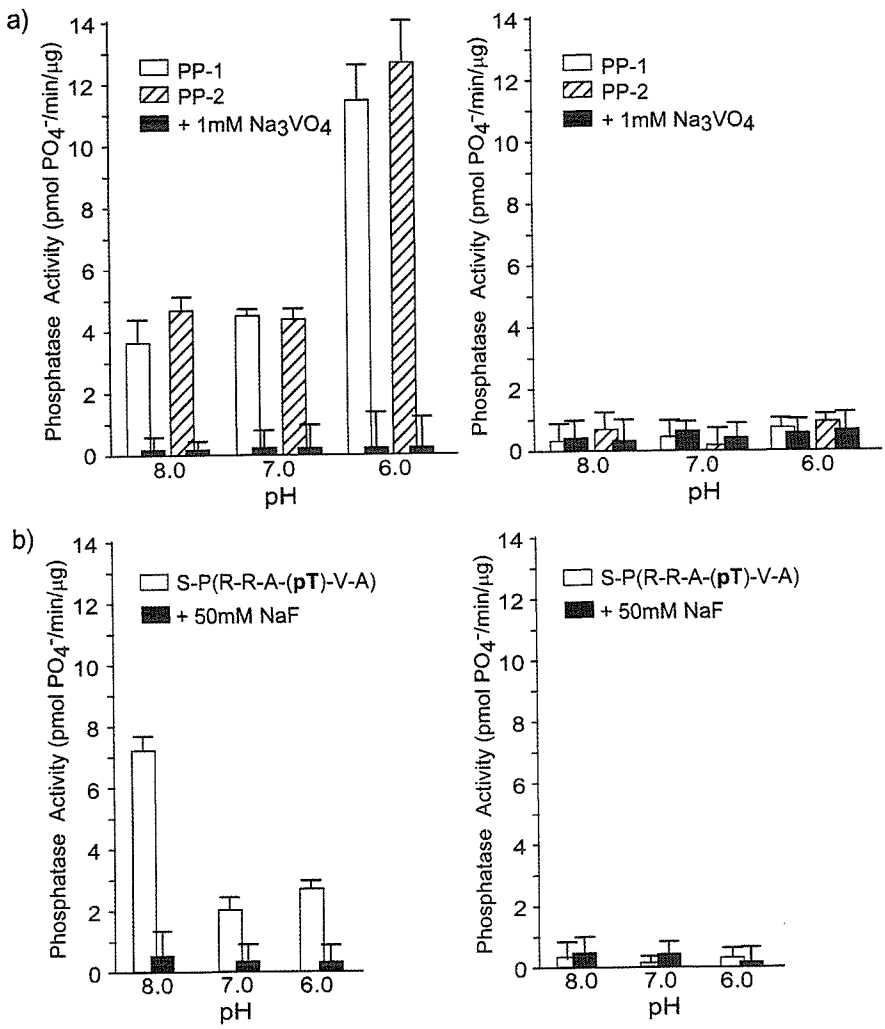

Fig. 2. Phosphatase activities of GST-DDSP. The sequence encoding GST-fused DDSP was ligated into the baculovirus expression vector and expressed in SF-9 cells. (a) Phosphotyrosine phosphatase activity of DDSP (left panel). PP-1 (open column) and PP-2 (dashed column) are 2 different kinds of phosphotyrosine substrate supplied by the manufacturer. Sodium vanadate (Na_3VO_4) is a PTP-specific inhibitor. The phosphatase activity was measured in the absence (open or dashed column) or presence (filled column) of 1 mM Na_3VO_4 and is shown as pmol phosphate released/min/μg of enriched cytosol after passage through a GST-affinity column. The right panel represents the activity of the sample from cells transfected with an empty vector plasmid. (b) Phosphothreonine phosphatase activity of DDSP (left panel). S-P is a phosphothreonine substrate. Sodium fluoride (NaF) is a serine/threonine phosphatase-specific inhibitor. The phosphatase activity was measured in the absence (open) or presence (filled column) of 50 mM NaF. The right panel represents the activity of the sample from cells transfected with an empty vector plasmid.

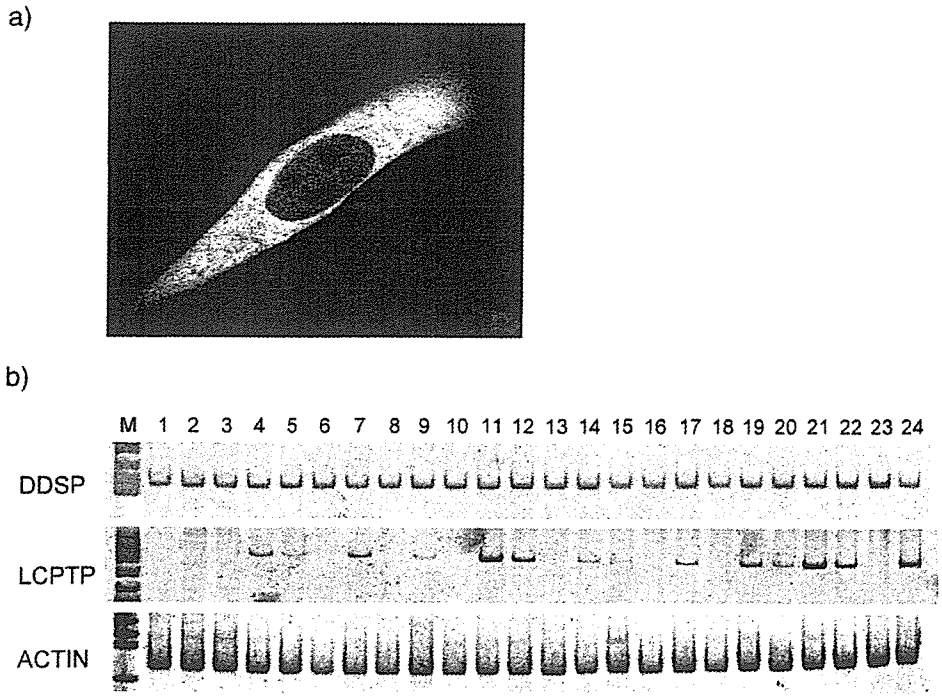

Fig. 3. Subcellular and tissue distribution of DDSP. (a) Cytoplasmic localization of DDSP. The DDSP cDNA sequence was ligated in-frame into pEGFP, transfected into COS7 cells and then subjected to a confocal microscopic analysis. (b) Tissue distribution of DDSP and LCPTP/HePTP. The 2 sequence specific sets of primers for DDSP (top panel) or LCPTP/HePTP (middle panel) were used for RT-PCR. The bottom panel represents the RT-PCR amplifying β-actin mRNA. Lanes are 1: brain; 2: heart; 3: kidney; 4: spleen; 5: liver; 6: colon; 7: lung; 8: small intestine; 9: skeletal muscle; 10: stomach; 11: testis; 12: placenta; 13: salivary gland; 14: thyroid; 15: adrenal; 16: pancreas; 17: ovary; 18: uterus; 19: prostate; 20: skin; 21: lymphocyte; 22: bone marrow; 23: fetal brain; 24: fetal liver.

fected cells with DHEA or treatment of the transfected PEER with or without PMA and A23187 did not significantly change the homogeneous cytoplasmic distribution of GFP-fluorescence (data not shown). Taken together with the observations of the DSP activities, these results indicated that 1–20 encoded a novel member of the cytoplasmic DSP family. We tentatively named this novel DSP DHEA-enhanced DSP (DDSP).

3.4. Profiles of tissue distribution, PMA/A23187 induction and hormonal regulation of DDSP mRNA

To discriminate the mRNA expression of DDSP (full-length 1–20) as potentially DSP from those of tissue-specific LCPTP/HePTP, we designed 2 sets of primers for RT-PCR experiments: one to amplify the sequence specific to DDSP and another specific to LCPTP/HePTP (Fig. 1b). Using these 2 sets of primers, we investigated the tissue distribution and the response to PMA/A23187 or hormonal stimulation. In strong contrast to the restricted tissue distribution of LCPTP/HePTP mRNA preferentially expressed in hematopoietic tissues (and in testis at RT-PCR level), the basal expression of DDSP mRNA was observed by RT-PCR at a similar expression level in all types of human tissues examined (Fig. 3b).

In PEER cells without PMA/A23187 stimulation, the basal expression level (standardized by the fragment length and β-actin expression) of DDSP mRNA was about 20 to 30% of that of LCPTP/HePTP. PMA/A23187 treatment rapidly increased the DDSP mRNA expression within 1 h and then reached a maximum level (5- to 7-fold) at 3 h poststimulation. 100 nM DHEA further increased the DDSP mRNA level by 2.5- to 3-fold at 3 h poststimulation (Fig. 4a). On the other hand, LCPTP/HePTP-specific RT-PCR showed a constitutive expression even in the untreated PEER cells, and PMA/A23187 stimulation with or without DHEA did not significantly alter the expression (Fig. 4b). Costimulation with either 100 nM dexamethasone (DEX), 1 μM DHEA sulfate (DHEAS) or 10 nM dihydrotestosterone (DHT) did not exert the reproducible induction of DDSP mRNA level in the repeated experiments, while the 10 nM 17β-estradiol (E2) treatment sometimes slightly repressed the PMA/A23187-induced DDSP expression. These steroid hormones, including DHEA, did not affect the mRNA levels of LCPTP/HePTP. In Fig. 4c and d, representative results of RT-PCR experiments were shown.

3.5. Interaction of DDSP with the MAPK cascade

To observe the interactions of DDSP with MAPK, we transfected a plasmid expressing a flag-DDSP fusion product into NIH3T3 mouse fibroblasts and then tested the binding of DDSP with activated endogenous ERK1/2, p38-MAPK or JNK by immunocoprecipitation. Western blotting showed that DDSP specifically bound to phosphorylated p38-MAPK activated by hyperosmotic 0.5M NaCl stimulation, but not to

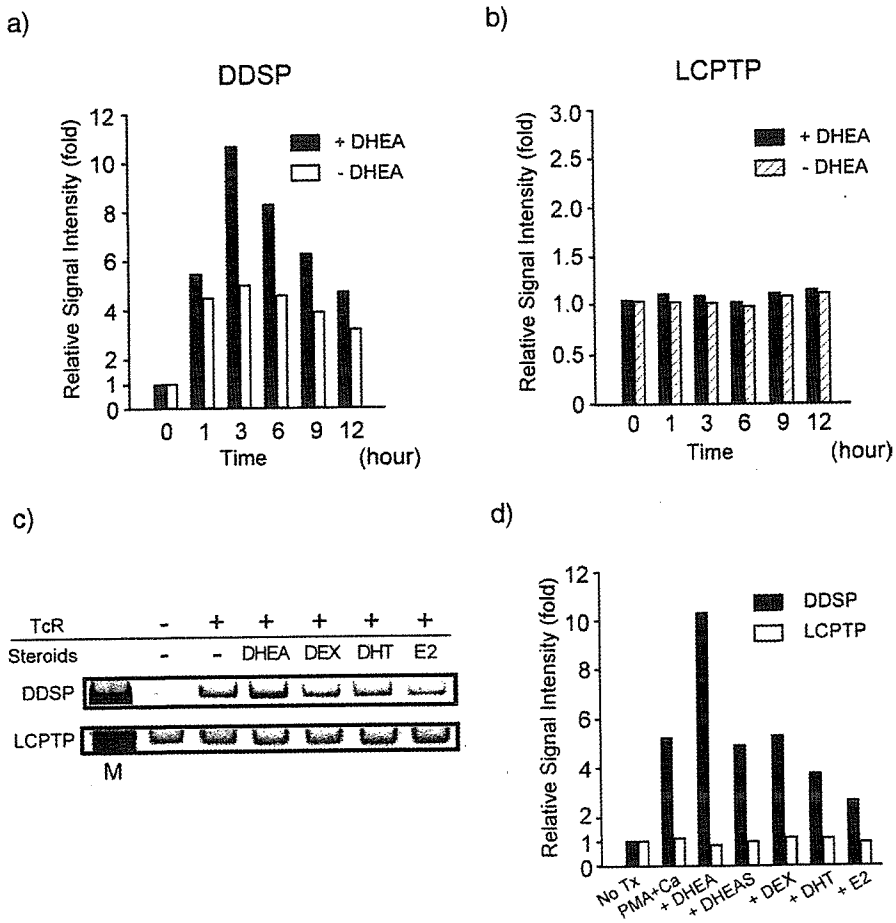

Fig. 4. The differential profiles of mRNA induction between DDSP and LCPTP/HePTP. The same primer set used in Fig. 3b was used for the RT-PCR. (a) The effect of a physiological concentration (100 nM) of DHEA on the expression of DDSP in TcR-activated PEER cells. PEER cells were stimulated by PMA and calcium ionophore A23187 with (filled bar) or without (open bar) DHEA. The relative induction values compared with the basal mRNA expression with no PMA/A23187 treatment, standardized by β-actin expression, are expressed as the-fold induction. (b) Effect of 100 nM DHEA on the expression of LCPTP/HePTP in TcR-activated PEER cells. PEER cells were stimulated as described above. The relative induction values are expressed as in Panel (a). Filled bars: with DHEA; hatched bars: without DHEA. (c) Effects of various steroid hormones on the mRNA expression of DDSP or LCPTP/HePTP. Representative results of the RT-PCR experiments are shown. The PEER cells were treated with PMA and calcium ionophore A23187 in the absence of any steroid hormones, or in the presence of 100 nM DHEA (DHEA), 100 nM dexamethasone (DEX), 10 nM dihydrotestosterone (DHT), or 1 nM 17β-estradiol (E2). The RNAs were extracted after 3 h of treatment and then subjected to semiquantitative RT-PCR using a set of primers specific for DDSP (upper panel) or LCPTP/HePTP (lower panel). (d) Schematic representation of the effects of the various steroid hormones. In this experiment, treatment with 1 μM of DHEA-sulfate (DHEAS) was included. The relative induction of each sequence in the PEER cells compared with the basal mRNA expression with no treatment (No Tx) is expressed as the-fold induction. The PEER cells were treated with PMA and calcium ionophore A23187 in the absence of any steroid hormones (PMA+Ca) or in the presence of 100 nM DHEA (DHEA), 1 μM DHEAS (DHEAS), 100 nM dexamethasone (DEX), 10 nM dihydrotestosterone (DHT) or 1 nM 17β-estradiol (E2), respectively. Filled bars: DDSP mRNA; open bars: LCPTP/HePTP mRNA.

activated ERK1/2 or JNK (Fig. 5a and b). This finding also suggested that the N-terminal 13 aa residues of DDSP (corresponding to aa residues 49–61 of LCPTP) were required for and enough for P38-MAPK-binding.

The inactivation of the phosphorylated p38-MAPK by DDSP was shown by the dephosphorylation of the phosphorylated p38-MAPK. DDSP specifically dephosphorylated the endogenous p38-MAPK, activated by hyperosmotic stimulation using 0.5 M NaCl, in NIH3T3 cells that were transiently transfected with plasmids expressing flag-tagged DDSP, while the phosphorylated ERK or JNK were not dephosphorylated (Fig. 6a). The p38-MAPK-specific inactivation was further confirmed using the pMACS system that can select transfected cells from untransfected cells and can thus enrich the transfected cells to nearly 80% after passage through an affinity column. The expression of the DDSP protein dephosphorylated the endogenous p38-MAPK activated by 0.4 M sorbitol hyperosmotic treatment, but not ERK activated by PMA treatment, in the cells selected after the enrichment (Fig. 6b). Taken together, these results indicated that DDSP inactivates the MAPK cascade in a p38-MAPK-specific fashion.

4. Discussion

To clarify the action of DHEA on a molecular basis, a comparison of the cellular phenotypes between the DHEA-

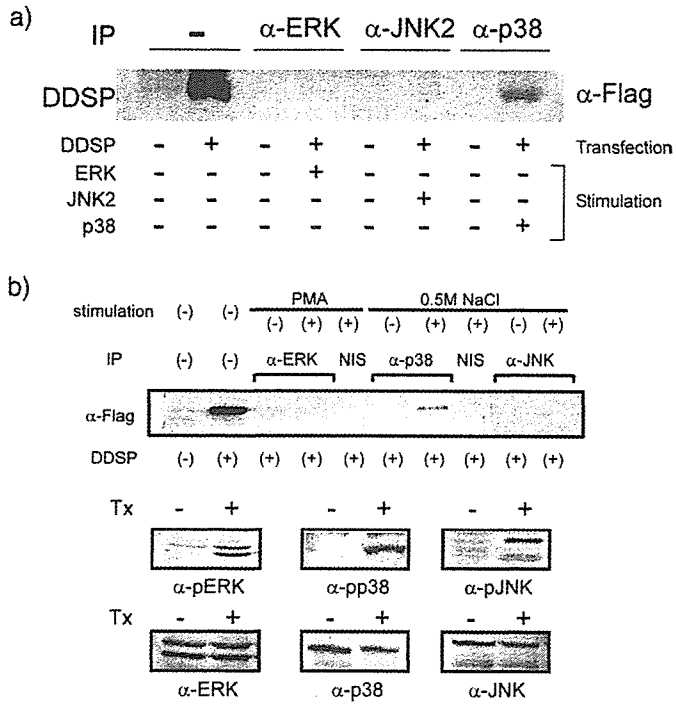

Fig. 5. Immunocoprecipitation of DDSP with ERK, p38 or JNK. (a) NIH3T3 cells transfected with a plasmid expressing flag-tagged DDSP were treated with 0.5 M NaCl for 20 min (for p38 and JNK) or with 50 ng/ml of PMA for 15 min after incubation in a serum free medium for 15 h (for ERK). The endogenous ERK, p-38 or JNK in the whole cell lysates from the treated cells was immunoprecipitated with an anti-ERK, -p38 or -JNK antibody, respectively, and then Western blotting was performed using an anti-flag antibody. DDSP specifically interacts with the endogenous phosphorylated p38-MAPK. (b) Immunoprecipitation and Western blot were performed as in Panel (a) (top panel). NIS: non-immune serum. In the middle and bottom panels, the three pairs of whole cell lysates used for the immunoprecipitations in the top panel were probed to confirm the activation of each MAPK, using antibodies against phosphorylated MAPKs (middle panels: anti-pERK, anti-pp38, anti-pJNK) or total MAPKs (bottom panels: anti-ERK, anti-p38, anti-JNK). Tx: PMA-treatment for the activation of ERK or 0.5 M NaCl treatment for the activation of p38- or JNK-MAPK.

treated and untreated cells led to the isolation of the p38 MAPK phosphatase, DDSP. We demonstrated that this novel member of the PTPN7 locus-derived family was a candidate for one of the target genes of DHEA. One explanation for the biological action of DHEA is that DHEA exerts its functions after being biotransformed into biologically more active androgens and estrogens in either the peripheral tissues or the target cells (intracrine mechanism) [23]. In contrast, the superinduction effect of DHEA on the DDSP mRNA level was specific according to the results shown in Fig. 4. As one of the broad range of actions caused by DHEA, DHEA(-S) has been used for some collagen disease as adjunctive treatment expecting the immune modulating action [24–27] (for review). In this regard, the lymphocytes from the periphery of systemic lupus erythematosus (SLE) patients had a more activated p38 MAPK, as well as ERK or JNK, status immediately ex vivo when compared with lymphocytes from the periphery of normal individuals [28].

We propose a mechanism to explain, at least in part, this immune modulating action, namely that DHEA exerts the anti-inflammatory action by directly suppressing the p38-MAPK cascade. Recently, p38-MAPK has received much attention as a potential drug target for diseases such as rheumatoid arthritis, endotoxic shock, inflammatory bowel disease, osteoporosis and many others [29]. Our findings suggest that DHEA augments the negative feedback regulation of MAPK cascades that have become overactivated due to stress or cytokine signals via a specific set of MAPK phosphatases in many human tissues. In the vascular smooth muscle cell, p38-MAPK activation by PDGF is inhibited by low molecular weight PTPs, thus suggesting that MAPK phosphatases are important negative regulators for the vascular smooth muscle cell growth and migration processes leading to the progression of atherosclerosis [8,9,30]. Apart from the action on the MAPK cascade, it has been demonstrated that DHEA inhibits the nuclear translocation of nuclear factor-κB (NF-κB) probably due to the induction of peroxisome via the peroxisome proliferator activated receptor α (PPARα) [31], or that DHEA inhibits the binding of transcription factor activator protein-1 (AP-1) to DNA [32], thus exerting the anti-inflammatory action. To date, no receptor for DHEA or DHEAS has yet been cloned. The presence of cytoplasmic DHEA binding activity has been demonstrated in human peripheral blood monocytes [7], vascular smooth muscle cell [9] and human T lymphocytes [16], although according to the human genome project, it seems unlikely that a classical steroid hormone receptor-type DHEA receptor exists. Interestingly, Liu et al. reported the existence of the putative membrane receptor for DHEA [33]. DHEA may directly exert its

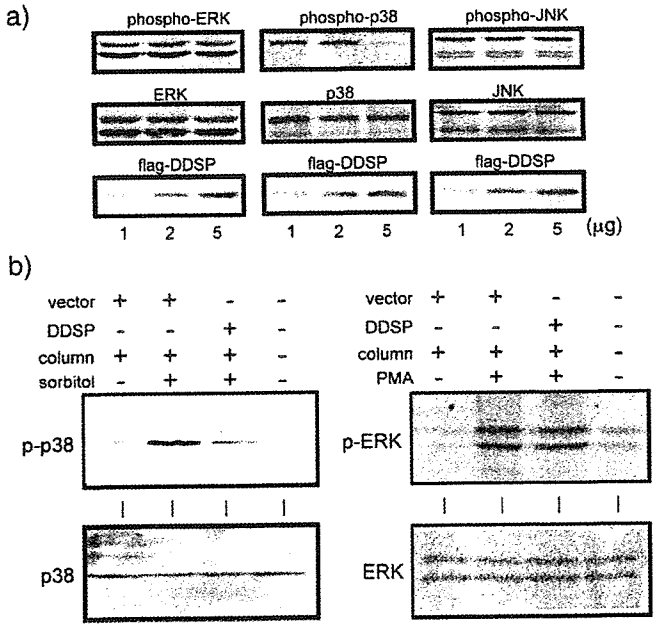

Fig. 6. DDSP dephosphorylates p38-MAPK. (a) Phosphatase activities of DDSP on ERK, p38 or JNK. NIH3T3 cells were transfected with 1, 2 or 5 μg of a plasmid expressing flag-tagged DDSP (left lane, middle lane and right lane, respectively, in each panel). The total amounts of the transfected plasmids were kept constant by adding the empty vector plasmid. The transfected cells were treated as in Fig. 5, and then the whole cell lysates were subjected to Western blotting. The antibodies were raised against phosphorylated (phospho-) MAPKs (top panels), total MAPKs (middle panels) or flag (bottom panels). (b) pMACS experiment showing the p38-MAPK-specific dephosphorylation. NIH3T3 cells were transfected in 10 cm dishes with 20 μg of pMACS-DDSP (DDSP), or pMACSKkII vector (vector) as a control. The transfected cells were enriched after column separation and then treated with 0.4 M sorbitol for 20 min to activate p38-MAPK or with 50 ng/ml PMA to activate ERK. Western blotting was performed using an antibody against phosphorylated p38-MAPK (upper left) or ERK (upper right) (shown as p-p38 and p-ERK, respectively) or total p38-MAPK (lower left) or ERK (lower right) (shown as p38 and ERK, respectively). In this experiment, the column passage alone mildly activated p38-MAPK and caused the basal level phosphorylation of p38-MAPK. The expression of DDSP specifically inactivated the p38-MAPK to the basal level.

action not through the nuclear receptor but through the signal transduction system, such as MAPK system, activated by membrane-type receptors.

The MAPK cascade is regulated by both the phosphorylation and dephosphorylation of the members of the cascade. LCPTP/HePTP has been shown to act as a phosphotyrosine-specific phosphatase for both ERK (ERK2) and p38-MAPK [34,35], and one report showed HePTP as the ERK2-specific phosphatase in the myelogenous leukemia cell line K562 [36]. While LCPTP/HePTP does not dephosphorylate phosphoserine/phosphothreonine residues in ERK1/2 [34], recent findings have revealed that a subfamily of PTP dephosphorylate not only the phosphotyrosine but also the phosphoserine/phosphothreonine residue, and was thus called DSP [37]. When we tested whether or not the DDSP protein possesses phosphatase activities for the phosphoserine/phosphothreonine residue, the DDSP protein also caused a rapid loss of the phosphate from the phosphothreonine as well as from the phosphotyrosine. These results indicated that the DDSP might play a role as a DSP in vivo.

Each DSP or PTP has a restricted subcellular localization [37] (for review), while LCPTP/HePTP has been shown to localize in the cytoplasm (cytoplasmic PTP) as well [38]. DDSP was cytoplasmic as well as LCPTP/HePTP. In contrast, the mRNA profiles of the tissue distribution and the response to MAPK cascade stimulation and steroid hormone treatment were different between DDSP and LCPTP/HePTP, while DDSP was highly homologous to LCPTP/HePTP. Although the mRNA expression of LCPTP/HePTP has previously been shown to be inducible, the RT-PCR experiments using specific sets of primers suggested that the expression of LCPTP/HePTP was constitutive while the actual inducible sequence could be that of DDSP. While mRNA levels in mouse lymphocytes, detected by Northern blots, increased upon stimulation with phytohemagglutinin, lipopolysaccharide, concanavalin A, or anti-CD3 [20], the HePTP protein was present even in resting cells, and its amount increased slightly [34]. The differential mRNA expression between DDSP and LCPTP/HePTP might be due to, though not to be tested yet, the differential promoter usage.

In addition, at the protein level, the substrate specificity was different between DDSP and LCPTP/HePTP. LCPTP/HePTP binds to both ERKs and p38-MAPK through a kinase-interaction motif (KIM) located at the N-terminus of the protein and inactivates them by dephosphorylating the critical phosphotyrosine residue in their activation loop, thus playing a negative role in the TcR signaling pathway [39]. Furthermore, the binding of HePTP to ERK or p38-MAPK is in a phosphorylation-independent fashion [34]. HePTP has previously been shown to interact with both ERK1/2 and p38-MAPK via the 40 aa of the N-terminus sequence [34]. The aa residues 1 to 40 of HePTP corresponded to aa residues 22 to 61 of LCPTP (Fig. 1b). In particular, Arg41 and Arg42 play a crucial role in ERK binding [35]. DDSP lacked the first 48 aa stretch (including Arg41 and Arg42) of LCPTP required for ERK1/2 binding, while the following aa sequence was highly conserved, except for 1 aa residue (Val 220, bold line in Fig. 1b) in addition to the unique 11 aa stretch at the C′ -terminus end (Fig. 1a). This may contribute to why DDSP specifically bound to and inactivated phosphorylated p38-MAPK. To date, only one molecule, Wip1, which is induced in response to ionizing radiation in a p53-dependent manner, has been shown to be a p38-specific MAPK phosphatase [40,41]. Our present study suggested the complexity of the gene regulation in the PTPN7 locus. By the mechanisms of alternative splicing and possible differential promoter usage, PTPN7 may encode at least 3 protein phosphatases: one is the inducible DDSP specifically inactivating p38-MAPK and the others are constitutively expressed PTPs inactivating both ERK and p38-MAPK.

Acknowledgements

We would like to thank Otsuka Pharmaceutical Co. Ltd., Japan, for valuable discussions and help during the SSH screening.

References

[1] R.J. Davis, The mitogen-activated protein kinase signal transduction pathway, J. Biol. Chem. 268 (1993) 14553–14556.

[2] Z. Galcheva-Gargova, B. Derijard, I.H. Wu, R.J. Davis, An osmosensing signal transduction pathway in mammalian cells, Science 265 (1994) 806–808.

[3] J.M. Kyriakis, P. Banerjee, E. Nikolakaki, T. Dai, E.A. Rubie, M.F. Ahmad, J. Avruch, J.R. Woodgett, The stress-activated protein kinase subfamily of c-*Jun* kinases, Nature 369 (1994) 156–160.

[4] E. Cano, L.C. Mahadevan, Parallel signal processing among mammalian MAPKs, Trends Biochem. Sci. 20 (1995) 117–122.

[5] R. Seger, E.G. Krebs, The MAPK signaling cascade, FASEB J. 9 (1995) 726–735.

[6] S. Tamura, M. Hanada, M. Ohnishi, K. Katsura, M. Sasaki, T. Kobayashi, Regulation of stress-activated protein kinase signaling pathways by protein phosphatases, Eur. J. Biochem. 269 (2002) 1060–1066.

[7] J.A. McLachlan, C.D. Serkin, O. Bakouche, Dehydroepiandrosterone modulation of lipopolysaccharide-stimulated monocyte cytotoxicity, J. Immunol. 156 (1996) 328–335.

[8] T. Yoshimata, A. Yoneyama, Y. Jin-no, N. Tamai, Y. Kamiya, Effects of dehydroepiandrosterone on mitogen-activated protein kinase in human aortic smooth muscle cells, Life Sci. 65 (1999) 431–440.

[9] M.R. Williams, S. Ling, T. Dawood, K. Hashimura, A. Dai, H. Li, J.P. Liu, J.W. Funder, K. Sudhir, P.A. Komesaroff, Dehydroepiandrosterone inhibits human vascular smooth muscle cell proliferation independent of ARs and ERs, J. Clin. Endocrinol. Metab. 87 (2002) 176–181.

[10] A.J. Morales, J.J. Nolan, J.C. Nelson, S.S. Yen, Effects of replacement dose of dehydroepiandrosterone in men and women of advancing age, J. Clin. Endocrinol. Metab. 78 (1994) 1360–1367.

[11] F. Labrie, P. Diamond, L. Cusan, J.L. Gomez, A. Belanger, B. Candas, Effect of 12-month dehydroepiandrosterone replacement therapy on bone, vagina, and endometrium in postmenopausal women, J. Clin. Endocrinol. Metab. 82 (1997) 3498–3505.

[12] W. Arlt, F. Callies, J.C. van Vlijmen, I. Koehler, M. Reincke, M. Bidlingmaier, D. Huebler, M. Oettel, M. Ernst, H.M. Schulte, B. Allolio, Dehydroepiandrosterone replacement in women with adrenal insufficiency, N. Engl. J. Med. 341 (1999) 1013–1020.

[13] E.E. Baulieu, G. Thomas, S. Legrain, N. Lahlou, M. Roger, B. Debuire, V. Faucounau, L. Girard, M.P. Hervy, F. Latour, M.C. Leaud, A. Mokrane, H. Pitti-Ferrandi, C. Trivalle, O. de Lacharriere, S. Nouveau, B. Rakoto-Arison, J.C. Souberbielle, J. Raison, Y. Le Bouc, A. Raynaud, X. Girerd, F. Forette, Dehydroepiandrosterone (DHEA), DHEA sulfate, and aging: contribution of the DHEAge Study to a sociobiomedical issue, Proc. Natl. Acad. Sci. U. S. A. 97 (2000) 4279–4284.

[14] H. Nawata, T. Yanase, K. Goto, T. Okabe, K. Ashida, Mechanism of action of anti-aging DHEA-S and the replacement of DHEA-S, Mech. Ageing Dev. 123 (2002) 1101–1106.

[15] Z. Ravid, N. Goldblum, R. Zaizov, M. Schlesinger, T. Kertes, J. Minowada, W. Verbi, M. Greaves, Establishment and characterization of a new leukaemic T-cell line (Peer) with an unusual phenotype, Int. J. Cancer 25 (1980) 705–710.

[16] T. Okabe, M. Haji, R. Takayanagi, M. Adachi, K. Imasaki, F. Kurimoto, T. Watanabe, H. Nawata, Up-regulation of high-affinity dehydroepiandrosterone binding activity by dehydroepiandrosterone in activated human T lymphocytes, J. Clin. Endocrinol. Metab. 80 (1995) 2993–2996.

[17] J.N. Siegel, R.D. Klausner, U.R. Rapp, L.E. Samelson, T cell antigen receptor engagement stimulates c-raf phosphorylation and induces c-raf-associated kinase activity via a protein kinase C-dependent pathway, J. Biol. Chem. 265 (1990) 18472–18480.

[18] M. Izquierdo, S. Bowden, D. Cantrell, The role of Raf-1 in the regulation of extracellular signal-regulated kinase 2 by the T cell antigen receptor, J. Exp. Med. 180 (1994) 401–406.

[19] M. Adachi, M. Sekiya, M. Isobe, Y. Kumura, Z. Ogita, Y. Hinoda, K. Imai, A. Yachi, Molecular cloning and chromosomal mapping of a human protein–tyrosine phosphatase LC-PTP, Biochem. Biophys. Res. Commun. 186 (1992) 1607–1615.

[20] B. Zanke, H. Suzuki, K. Kishihara, L. Mizzen, M. Minden, A. Pawson, T.W. Mak, Cloning and expression of an inducible lymphoid-specific, protein tyrosine phosphatase (HePTPase), Eur. J. Immunol. 22 (1992) 235–239.

[21] M. Saxena, S. Williams, K. Tasken, T. Mustelin, Crosstalk between cAMP-dependent kinase and MAP kinase through a protein tyrosine phosphatase, Nat. Cell Biol. 1 (1999) 305–311.

[22] M. Adachi, T. Miyachi, M. Sekiya, Y. Hinoda, A. Yachi, K. Imai, Structure of the human LC-PTP (HePTP) gene: similarity in genomic organization within protein-tyrosine phosphatase genes, Oncogene 9 (1994) 3031–3035.

[23] F. Labrie, A. Belanger, J. Simard, L.-T. Van, C. Labrie, DHEA and peripheral androgen and estrogen formation: intracinology, Ann. N.Y. Acad. Sci. 774 (1995) 16–28.

[24] R.H. Derksen, Dehydroepiandrosterone (DHEA) and systemic lupus erythematosus, Semin. Arthritis Rheum. 27 (1998) 335–347.

[25] D.M. Chang, J.L. Lan, H.Y. Lin, S.F. Luo, Dehydroepiandrosterone treatment of women with mild-to-moderate systemic lupus erythematosus: a multicenter randomized, double-blind, placebo-controlled trial, Arthritis Rheum. 46 (2002) 2924–2927.

[26] M.A. Petri, R.G. Lahita, R.F. Van Vollenhoven, J.T. Merrill, M. Schiff, E.M. Ginzler, V. Strand, A. Kunz, K.J. Gorelick, K.E. Schwartz, Effects of prasterone on corticosteroid requirements of women with systemic lupus erythematosus: a double-blind, randomized, placebo-controlled trial, Arthritis Rheum. 46 (2002) 1820–1829.

[27] R.F. van Vollenhoven, Dehydroepiandrosterone in systemic lupus erythematosus, Rheum. Dis. Clin. North Am. 26 (2000) 349–362.

[28] A.C. Grammer, R. Fischer, O. Lee, X. Zhang, P.E. Lipsky, Flow cytometric assessment of the signaling status of human B lymphocytes from normal and autoimmune individuals, Arthritis Res. Ther. 6 (2004) 28–38 (Electronic publication 2004 Feb 2005).

[29] R.L. Thurmond, S.A. Wadsworth, P.H. Schafer, R.A. Zivin, J.J. Siekierka, Kinetics of small molecule inhibitor binding to p38 kinase, Eur. J. Biochem. 268 (2001) 5747–5754.

[30] H. Shimizu, M. Shiota, N. Yamada, K. Miyazaki, N. Ishida, S. Kim, H. Miyazaki, Low M(r) protein tyrosine phosphatase inhibits growth and migration of vascular smooth muscle cells induced by platelet-derived growth factor, Biochem. Biophys. Res. Commun. 289 (2001) 602–607.

[31] M.E. Poynter, R.A. Daynes, Peroxisome proliferator-activated receptor alpha activation modulates cellular redox status, represses nuclear factor-kappaB signaling, and reduces inflammatory cytokine production in aging, J. Biol. Chem. 273 (1998) 32833–32841.

[32] R. Dashtaki, A.R. Whorton, T.M. Murphy, P. Chitano, W. Reed, T.P. Kennedy, Dehydroepiandrosterone and analogs inhibit DNA binding of AP-1 and airway smooth muscle proliferation, J. Pharmacol. Exp. Ther. 285 (1998) 876–883.

[33] D. Liu, J.S. Dillon, Dehydroepiandrosterone activates endothelial cell nitric-oxide synthase by a specific plasma membrane receptor coupled to Galpha(i2,3), J. Biol. Chem. 277 (2002) 21379–21388 (Electronic publication 22002 Apr 21304).

[34] M. Saxena, S. Williams, J. Brockdorff, J. Gilman, T. Mustelin, Inhibition of T cell signaling by mitogen-activated protein kinase-

targeted hematopoietic tyrosine phosphatase (HePTP), J. Biol. Chem. 274 (1999) 11693–11700.

[35] M. Oh-hora, M. Ogata, Y. Mori, M. Adachi, K. Imai, A. Kosugi, T. Hamaoka, Direct suppression of TCR-mediated activation of extracellular signal-regulated kinase by leukocyte protein tyrosine phosphatase, a tyrosine-specific phosphatase, J. Immunol. 163 (1999) 1282–1288.

[36] S.M. Pettiford, R. Herbst, The MAP-kinase ERK2 is a specific substrate of the protein tyrosine phosphatase HePTP, Oncogene 19 (2000) 858–869.

[37] M. Camps, A. Nichols, S. Arkinstall, Dual specificity phosphatases: a gene family for control of MAP kinase function, FASEB J. 14 (2000) 6–16.

[38] A. Gjorloff-Wingren, M. Saxena, S. Han, X. Wang, A. Alonso, M. Renedo, P. Oh, S. Williams, J. Schnitzer, T. Mustelin, Subcellular localization of intracellular protein tyrosine phosphatases in T cells, Eur. J. Immunol. 30 (2000) 2412–2421.

[39] M. Saxena, S. Williams, J. Gilman, T. Mustelin, Negative regulation of T cell antigen receptor signal transduction by hematopoietic tyrosine phosphatase (HePTP), J. Biol. Chem. 273 (1998) 15340–15344.

[40] M. Fiscella, H. Zhang, S. Fan, K. Sakaguchi, S. Shen, W.E. Mercer, G.F. Vande Woude, P.M. O'Connor, E. Appella, Wip1, a novel human protein phosphatase that is induced in response to ionizing radiation in a p53-dependent manner, Proc. Natl. Acad. Sci. U. S. A. 94 (1997) 6048–6053.

[41] M. Takekawa, M. Adachi, A. Nakahata, I. Nakayama, F. Itoh, H. Tsukuda, Y. Taya, K. Imai, p53-inducible wip1 phosphatase mediates a negative feedback regulation of p38 MAPK-p53 signaling in response to UV radiation, EMBO J. 19 (2000) 6517–6526.

Available online at www.sciencedirect.com
SCIENCE DIRECT®
Biochemical and Biophysical Research Communications 329 (2005) 177–181
BBRC
www.elsevier.com/locate/ybbrc

Glucocorticoid suppresses the canonical Wnt signal in cultured human osteoblasts

Keizo Ohnaka[a,*], Mizuho Tanabe[a], Hisaya Kawate[a], Hajime Nawata[b], Ryoichi Takayanagi[a]

[a] *Department of Geriatric Medicine, Graduate School of Medical Sciences, Kyushu University, 3-1-1 Maidashi, Higashi-ku, Fukuoka 812-8582, Japan*
[b] *Department of Medicine and Bioregulatory Science, Graduate School of Medical Sciences, Kyushu University, 3-1-1 Maidashi, Higashi-ku, Fukuoka 812-8582, Japan*

Received 22 January 2005

Abstract

To explore the mechanism of glucocorticoid-induced osteoporosis, we investigated the effect of glucocorticoid on canonical Wnt signaling that emerged as a novel key pathway for promoting bone formation. Wnt3a increased the T-cell factor (Tcf)/lymphoid enhancer factor (Lef)-dependent transcriptional activity in primary cultured human osteoblasts. Dexamethasone suppressed this transcriptional activity in a dose-dependent manner, while 1,25-dihydroxyvitamin D3 increased this transcriptional activity. LiCl, an inhibitor of glycogen synthase kinase-3β, also enhanced the Tcf/Lef-dependent transcriptional activity, which was, however, not inhibited by dexamethasone. The addition of anti-dickkopf-1 antibody partially restored the transcriptional activity suppressed by dexamethasone. Dexamethasone decreased the cytosolic amount of β-catenin accumulated by Wnt3a and also inhibited the nuclear translocation of β-catenin induced by Wnt3a. These data suggest that glucocorticoid suppresses the canonical Wnt signal in cultured human osteoblasts, partially through the enhancement of the dickkopf-1 production.

Keywords: Glucocorticoid; Wnt; Dickkopf-1; Osteoblast; Osteoporosis

Osteoporosis is one of the most frequent and serious side effects of long-term glucocorticoid therapy [1]. Glucocorticoids have profound effects on bone metabolism [2]. Glucocorticoid excess increases bone resorption and decreases bone formation; consequently rapid bone loss occurs. Nowadays, a direct inhibition of osteoblast activity by glucocorticoids is the most favored principal mechanism of glucocorticoid-induced osteoporosis [1–3]. However, detailed mechanism by which they inhibit osteoblast function remains to be fully elucidated.

Recent progress uncovers the importance of Wnt signaling in skeletal biology [4,5]. The loss-of-function mutations in human LDL receptor-related protein 5 (LRP5) gene cause osteoporosis-pseudoglioma syndrome (OPPG) characterized by low bone mass and abnormal eye development, while the gain-of-function mutations in this gene give rise to high bone mass syndrome [6–8]. Furthermore, the LRP5 gene knockout mice show the phenotype of low bone mass resembling that of human OPPG [9]. These findings highlighted Wnt signaling as another key pathway involved in the regulation of postnatal bone mass.

The Wnt signal transduction comprises three intracellular pathways: the canonical pathway, the Wnt/planar-cell-polarity (PCP) pathway, and the Wnt/Ca^{2+} pathway [10,11]. Although which pathway is involved in bone formation remains to be fully elucidated, recent studies strongly suggest that the canonical pathway plays a central role in promoting bone formation [4,5,12]. Canonical Wnts bind to frizzled/LRP5 receptor complex, inactivate glycogen synthase kinase-3β

* Corresponding author. Fax: +81 92 642 6911.
E-mail address: oonaka@geriat.med.kyushu-u.ac.jp (K. Ohnaka).

(GSK-3β), and inhibit phosphorylation and consequential degradation of intracellular β-catenin [10,11]. Accumulated β-catenin translocates into the nucleus and activates target genes by a complex formed with transcription factors of the T-cell factor (Tcf)/lymphoid enhancer factor (Lef) family [10,11].

Wnt signals are extracellularly regulated by several secreted antagonists including secreted frizzled-related protein (sFRP), Cerberus, Wnt inhibitory factor-1 (WIF-1), and dickkopf (Dkk) [13]. We have reported that glucocorticoid enhances the expression of dickkopf-1 (Dkk-1) in cultured human osteoblasts [14]. We extended our exploration of the effect of glucocorticoid on Wnt signaling, and found that glucocorticoid suppresses the canonical Wnt signal, in part mediated by the enhancement of the Dkk-1 production, in cultured human osteoblasts.

Materials and methods

Materials. Eagle's α-MEM, penicillin, and streptomycin were obtained from Invitrogen (Carlsbad, CA). Fetal calf serum (FCS) was purchased from Sanko Junyaku (Tokyo, Japan). Dexamethasone, 17β-estradiol, dihydrotestosterone, 1,25-dihydroxyvitamin D3, LiCl, and goat immunoglobulin (IgG) were purchased from Sigma (St. Louis, MI). Anti-β-catenin monoclonal antibody and anti-Dkk-1 goat polyclonal antibody were purchased from Transduction Laboratories (Lexington, KY) and Santa Cruz Biotechnology (Santa Cruz, CA), respectively. All other reagents were of analytical grade.

Cell culture. Human osteoblasts were prepared from the bone fragments of femur neck as described previously [15]. The cells were grown in Eagle's α-MEM with 10% FCS, 100 mU/ml penicillin, and 100 mU/ml streptomycin. The Wnt3a-expressing cell line (L Wnt-3A cell) and the control cell line (L cell) were obtained from American Type Culture Collection (Manassas, VA). Wnt3a-conditioned medium (Wnt3a-CM) and the control-conditioned medium (C-CM) were harvested according to the manufacturer's instructions. Wnt3a-CM was used in experiments at 10% final concentration, which gave the maximal effect on the Tcf/Lef-dependent transcriptional activity in preliminary studies (data not shown).

Plasmid constructs. The entire coding region of human β-catenin was amplified by reverse transcriptase-polymerase chain reaction (RT-PCR) using KOD-plus DNA polymerase (Toyobo, Tokyo, Japan), confirmed by DNA sequencing, and subcloned into *ScaI*/*Bam*HI sites of pEGFP-C3 (Clontech, Palo Alto, CA) expression vector (designated as pEGFP-β-catenin). TOPflash, a Tcf-binding site reporter plasmid, was purchased from Upstate Biotechnology (Lake Placid, NY).

Transient transfection and reporter assay. Human osteoblasts were transiently transfected by means of calcium phosphate precipitation as described previously [14]. Reporter assay was performed by a dual luciferase assay kit (Promega, MI) according to the manufacturer's instructions.

Subcellular fractionation and immunoblot analysis. Subcellular fractionation and immunoblot analysis were performed essentially as described previously [15]. Soluble (cytosolic) proteins were subjected to sodium dodecyl sulfate–polyacrylamide gel electrophoresis (SDS–PAGE) and proteins in the gel were transferred to a Hybond ECL nitrocellulose membrane (Amersham Biosciences Corp., Piscataway, NJ) through electroblotting. For detection of β-catenin, blots were probed with an anti-β-catenin monoclonal antibody at a dilution of 1:1000. The protein concentration was determined by a BCA protein assay kit (Pierce, Rockford, IL).

Confocal laser microscopic imaging. Human osteoblasts were cultured in 35-mm glass-bottomed dishes (Asahi Techno Glass, Tokyo, Japan) and transfected with pEGFP-β-catenin plasmid vector. The cells were maintained in α-MEM supplemented with 10% charcoal-treated FCS for 24 h and observed with a confocal laser scanning microscope (LSM 510 META, Carl Zeiss, Jena, Germany) as described previously [16].

Statistical analysis. Data are expressed as means ± SD. Statistical analyses were performed with ANOVA followed by Fisher's protected least significant difference test. Significance was accepted at $P < 0.05$.

Results

To investigate the effect of glucocorticoid on canonical Wnt signaling, we first examined whether glucocorticoid would affect the Tcf/Lef-dependent transcriptional activity by a Tcf-reporter gene (luciferase) assay in cultured osteoblasts (Fig. 1A). In primary cultured human osteoblasts, the addition of Wnt3a-conditioned medium (Wnt3a-CM) enhanced the Tcf/Lef-dependent transcriptional activity (approximately 3.5-fold). Dexamethasone suppressed the Wnt3a-induced Tcf/Lef-dependent transcriptional activity in a dose-dependent manner, and dexamethasone at 10^{-7} M suppressed the Wnt3a-stimulated transcriptional activity to the unstimulated basal level.

We also examined the effect of other steroid hormones on the Tcf/Lef-dependent transcriptional activity (Fig. 1B). The addition of 17β-estradiol or dihydrotestosterone did not affect the transcriptional activity stimulated by Wnt3a. The addition of 1,25-dihydroxyvitamin D3 (10^{-7} M) enhanced the Wnt3a-induced reporter activity in cultured human osteoblasts. Furthermore, 1,25-dihydroxyvitamin D3 partially restored the suppressed Wnt3a-induced transcriptional activity by dexamethasone.

Wnt proteins enhance Tcf/Lef-dependent transcription by the canonical signal cascade, namely, the inhibition of GSK-3β, its consequential accumulation of cytosolic β-catenin, translocation of the accumulated β-catenin into the nucleus, and its activation of Tcf/Lef. Therefore, we examined whether or not dexamethasone would affect the intracellular β-catenin level in cultured human osteoblasts. As shown in Fig. 2, the addition of Wnt3a-CM increased the amount of cytosolic β-catenin protein in human osteoblasts. Co-treatment with dexamethasone (10^{-9}–10^{-7} M) dose-dependently decreased the cytosolic level of β-catenin and dexamethasone at 10^{-7} M almost completely reduced to the unstimulated basal level, which is parallel to the suppressive effect of dexamethasone on the reporter luciferase activity. When pEGFP-β-catenin was transfected into human osteoblasts, the GFP-β-catenin was localized most abundantly in the cytosol (Fig. 3). The addition of Wnt3a-CM translocated the GFP-β-catenin into the nucleus, however, co-treatment with

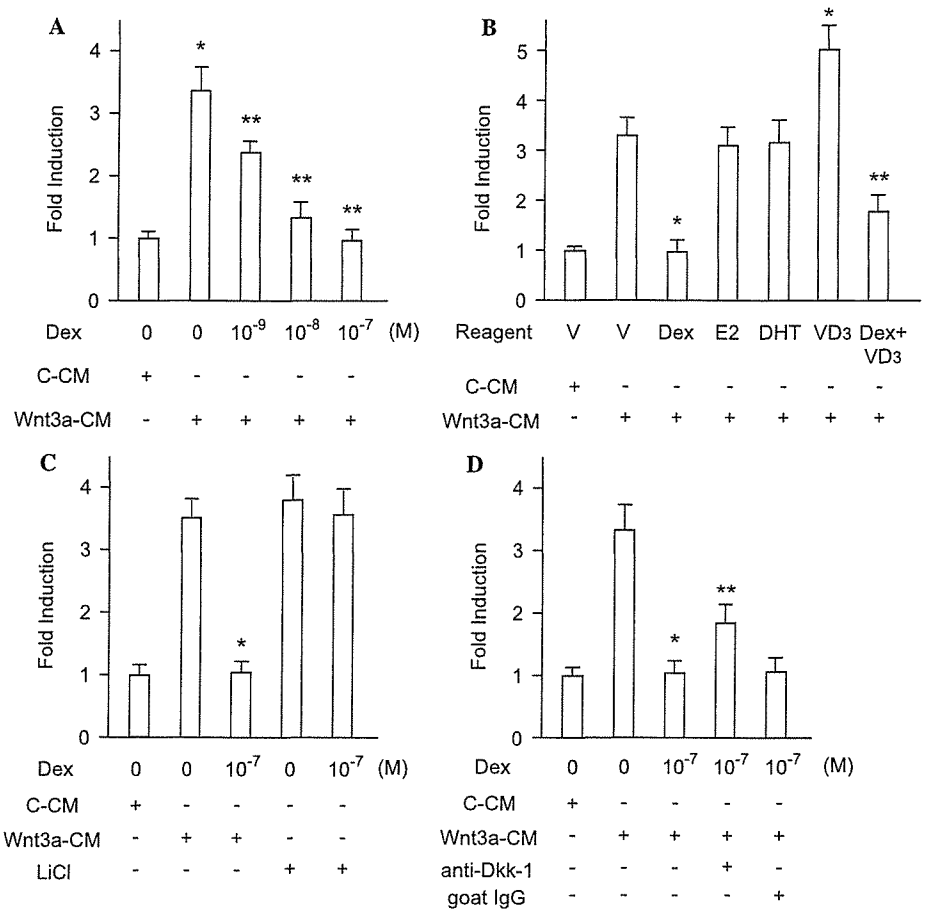

Fig. 1. Effects of Wnt3a, steroid hormones, LiCl, and anti-Dkk-1 antibody on the Tcf/Lef-dependent transcriptional activity in primary cultured human osteoblasts. Human osteoblasts were transfected with TOPflash plasmid vector, and incubated for 36 h with the control-conditioned medium (C-CM) or Wnt3a-conditioned medium (Wnt3a-CM) in the presence of vehicle (ethanol) or various reagents indicated. The reporter luciferase activity was expressed as fold over the activity of TOPflash with C-CM and vehicle. Data are expressed as means ± SD ($n = 4$). One representative data of three independent experiments are shown. (A) 10^{-9}–10^{-7} M dexamethasone (Dex). $^{*}P < 0.01$ vs. C-CM with vehicle. $^{**}P < 0.01$ vs. Wnt3a-CM with vehicle. (B) Vehicle (V, ethanol), 10^{-7} M dexamethasone (Dex), 10^{-7} M 17β-estradiol (E2), 10^{-7} M dihydrotestosterone (DHT), or 10^{-7} M 1,25-dihydroxyvitamin D3 (VD3). $^{*}P < 0.01$ vs. Wnt3a-CM with vehicle. $^{**}P < 0.05$ vs. Wnt3a-CM with Dex. (C) Twenty-five millimolar of LiCl in the presence of vehicle (ethanol) or 10^{-7} M dexamethasone (Dex). $^{*}P < 0.01$ vs. Wnt3a-CM with vehicle. (D) 10^{-7} M dexamethasone (Dex) in combination with anti-Dkk-1 goat polyclonal antibody (anti-Dkk-1) or non-immune goat IgG (goat IgG). $^{*}P < 0.01$ vs. Wnt3a-CM with vehicle. $^{**}P < 0.05$ vs. Wnt3a-CM with Dex.

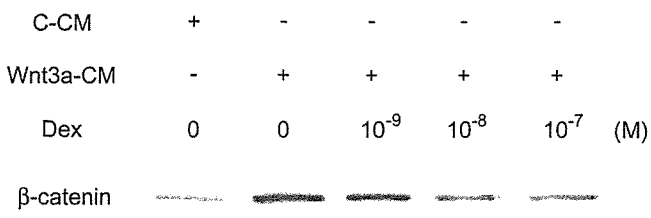

Fig. 2. Effect of dexamethasone on the level of the cytosolic β-catenin protein in primary cultured human osteoblasts. Human osteoblasts were incubated with the control-conditioned medium (control-CM) or Wnt3a-conditioned medium (Wnt3a-CM) in the presence of vehicle (ethanol) or 10^{-9}–10^{-7} M dexamethasone (Dex) for 24 h, and fractionated to soluble and particulate fractions. Soluble proteins (20 μg) were loaded in each lane and subjected to SDS–PAGE (7.5% separating gel). Immunoblot analyses were performed using a specific anti-β-catenin monoclonal antibody. Results shown are representative of three independent experiments.

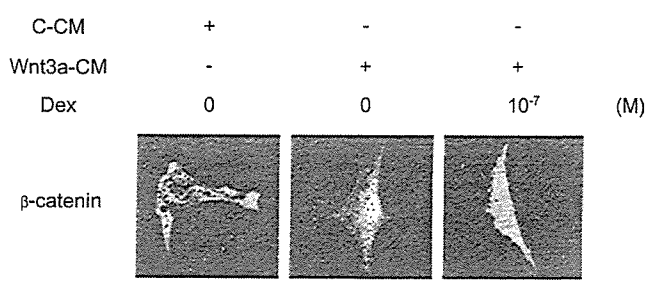

Fig. 3. Effect of dexamethasone on the localization of β-catenin in primary cultured human osteoblasts. Human osteoblasts were transfected with the pEGFP-β-catenin expression vector, and incubated for 24 h with the control-conditioned medium (control-CM) or Wnt3a-conditioned medium (Wnt3a-CM) in the presence of vehicle (ethanol) or 10^{-7} M dexamethasone (Dex). The cells were analyzed by laser confocal microscopy. A representative imaging of three independent experiments is shown (magnification, 100×).

dexamethasone at 10^{-7} M completely inhibited the nuclear translocation of cytosolic β-catenin (Fig. 3). These data suggest that dexamethasone suppressed the Tcf/Lef-dependent transcription through the canonical Wnt signaling cascade rather than by affecting via other signaling pathway(s) or inhibiting directly the Tcf/Lef expression in human osteoblasts.

To further assess the effect of dexamethasone on canonical Wnt signaling, we observed the effect of dexamethasone on the Tcf reporter activity in the presence of LiCl, an inhibitor of GSK-3β, in human osteoblasts (Fig. 1C). The addition of 25 mM LiCl increased the Tcf/Lef-dependent transcriptional activity comparable to that by Wnt3a-CM. However, this increase by LiCl was not suppressed by the treatment with dexamethasone at 10^{-7} M. Since glucocorticoid enhances the expression of Dkk-1, an antagonist of Wnt signaling in human osteoblast [14], we examined the involvement of Dkk-1 in suppressive effect of dexamethasone on canonical Wnt signaling. The addition of anti-Dkk-1-specific goat polyclonal antibody in part (35–45%) restored the suppression of Wnt3a-induced Tcf/Lef-dependent transcriptional activity by dexamethasone, while non-specific goat IgG had no effect on it (Fig. 1D).

Discussion

In the present study, we demonstrated that dexamethasone suppressed the Tcf/Lef-dependent canonical Wnt signaling pathway in primary cultured human osteoblasts. This effect was in part attributed to the increase of Dkk-1 expression by dexamethasone.

Glucocorticoid suppresses osteoblastic differentiation and proliferation by affecting multiple aspects of osteoblast function [1–3]. One well-known effect of glucocorticoid on osteoblast is the inhibition of the expression for Runx2/Cbfa1 [17], a crucial transcriptional factor for differentiation of osteoblast lineage [18]. Runx2/Cbfa1 promotes early osteoblast differentiation from undifferentiated mesenchymal cells, but rather inhibits late osteoblast maturation [18,19]. On the other hand, the Wnt signal plays an essential role in postnatal bone accrual in a Runx2/Cbfa1-independent manner [9]. Our data suggest that glucocorticoid at a therapeutic pharmacological dose may almost completely suppress the canonical Wnt signaling pathway promoting postnatal bone formation in human osteoblasts.

Dexamethasone did not affect the enhancement of Tcf/Lef-dependent transcriptional activity by LiCl, a GSK-3β inhibitor. Therefore, it is presumed that the dexamethasone affects canonical Wnt signaling through GSK-3β itself or upstream of GSK-3β. Indeed, it was reported that glucocorticoid activates GSK-3β and inhibits cell cycle progression in murine preosteoblastic MC3T3-E1 cells [20]. We have previously shown that glucocorticoid enhances the expression of Dkk-1, a secreted antagonist of Wnt signaling, in cultured human osteoblasts [14]. Treatment with anti-Dkk-1-specific antibody partially (approximately 40%) restored the suppression by dexamethasone of Wnt3a-induced Tcf/Lef-dependent transcriptional activity. Although there are several secreted antagonists of Wnt signaling [13] and we did not examine the involvement of other antagonists than Dkk-1 proteins, our data suggest that the inhibition of the canonical Wnt signal by glucocorticoid may be in part through the antagonistic effect of the enhanced Dkk-1 production in cultured human osteoblasts.

Interestingly, 1,25-dihydroxyvitamin D3 enhanced the Tcf/Lef-dependent transcriptional activity induced by Wnt3a in cultured human osteoblasts. Furthermore, 1,25-dihydroxyvitamin D3 restored the suppressed Wnt3a-induced transcriptional activity by dexamethasone. Previous study reported that the vitamin D receptor with its ligand inhibits β-catenin-Tcf/Lef-dependent gene transcription in colon carcinoma cells [21]. The vitamin D effect on Wnt signaling may be different by the types of cell and target genes, which will require further investigations. Active vitamin D metabolites are used for prevention and treatment of glucocorticoid-induced osteoporosis [22,23]. Besides the known effects of vitamin D3 on bone and mineral metabolism [23], the effect on Wnt signaling may contribute to the clinical effect of vitamin D3 for the treatment of osteoporosis.

LRP5 knockout mice show low bone mass due to decreased osteoblast proliferation [9], but the precise mechanism whereby the Wnt/LRP5 signal promotes bone formation remains to be fully clarified. However, given the significance of the canonical Wnt signaling pathway in postnatal control of bone formation, strong inhibition of this pathway by glucocorticoid may in part explain the impairment of osteoblastic function and bone formation induced by glucocorticoid excess. Our findings in this study and further investigations will provide clues to new strategies for the treatment of glucocorticoid-induced osteoporosis.

Acknowledgments

This work was supported in part by Grants-in-Aid for Scientific Research (B), Scientific Research (C) and Exploratory Research, and a grant for the 21st Century Center of Excellence (COE) Program (Kyushu University) from the Japanese Ministry of Education, Culture, Sports, Science and Technology.

References

[1] K.G. Saag, Glucocorticoid-induced osteoporosis, Endocrinol. Metab. Clin. North Am. 32 (2003) 135–157.

[2] E. Canalis, Clinical review 83: Mechanisms of glucocorticoid action in bone: Implications to glucocorticoid-induced osteoporosis, J. Clin. Endocrinol. Metab. 81 (1996) 3441–3447.
[3] S.C. Manolagas, R.S. Weinstein, New developments in the pathogenesis and treatment of steroid-induced osteoporosis, J. Bone Miner. Res. 14 (1999) 1061–1066.
[4] M.L. Johnson, K. Harnish, R. Nusse, W. Van Hul, LRP5 and Wnt signaling: A union made for bone, J. Bone Miner. Res. 19 (2004) 1749–1757.
[5] J.J. Westendorf, R.A. Kahler, T.M. Schroeder, Wnt signaling in osteoblasts and bone diseases, Gene 341 (2004) 19–39.
[6] Y. Gong, R.B. Slee, N. Fukai, G. Rawadi, S. Roman-Roman, A.M. Reginato, H. Wang, T. Cundy, F.H. Glorieux, D. Lev, M. Zacharin, K. Oexle, J. Marcelino, W. Suwairi, S. Heeger, G. Sabatakos, S. Apte, W.N. Adkins, J. Allgrove, M. Arslan-Kirchner, J.A. Batch, P. Beighton, G.C. Black, R.G. Boles, L.M. Boon, C. Borrone, H.G. Brunner, G.F. Carle, B. Dallapiccola, A. De Paepe, B. Floege, M.L. Halfhide, B. Hall, R.C. Hennekam, T. Hirose, A. Jans, H. Juppner, C.A. Kim, K. Keppler-Noreuil, A. Kohlschuetter, D. LaCombe, M. Lambert, E. Lemyre, T. Letteboer, L. Peltonen, R.S. Ramesar, M. Romanengo, H. Somer, E. Steichen-Gersdorf, B. Steinmann, B. Sullivan, A. Superti-Furga, W. Swoboda, M.J. van den Boogaard, W. Van Hul, M. Vikkula, M. Votruba, B. Zabel, T. Garcia, R. Baron, B.R. Olsen, M.L. Warman, LDL receptor-related protein 5 (LRP5) affects bone accrual and eye development, Cell 107 (2001) 513–523.
[7] L.M. Boyden, J. Mao, J. Belsky, L. Mitzner, A. Farhi, M.A. Mitnick, D. Wu, K. Insogna, R.P. Lifton, High bone density due to a mutation in LDL-receptor-related protein 5, N. Engl. J. Med. 346 (2002) 1513–1521.
[8] R.D. Little, J.P. Carulli, R.G. Del Mastro, J. Dupuis, M. Osborne, C. Folz, S.P. Manning, P.M. Swain, S.C. Zhao, B. Eustace, M.M. Lappe, L. Spitzer, S. Zweier, K. Braunschweiger, Y. Benchekroun, X. Hu, R. Adair, L. Chee, M.G. FitzGerald, C. Tulig, A. Caruso, N. Tzellas, A. Bawa, B. Franklin, S. McGuire, X. Nogues, G. Gong, K.M. Allen, A. Anisowicz, A.J. Morales, P.T. Lomedico, S.M. Recker, P. Van Eerdewegh, R.R. Recker, M.L. Johnson, A mutation in the LDL receptor-related protein 5 gene results in the autosomal dominant high-bone-mass trait, Am. J. Hum. Genet. 70 (2002) 11–19.
[9] M. Kato, M.S. Patel, R. Levasseur, I. Lobov, B.H. Chang, D.A. Glass, C. Hartmann, L. Li, T.H. Hwang, C.F. Brayton, R.A. Lang, G. Karsenty, L. Chan, Cbfa1-independent decrease in osteoblast proliferation, osteopenia, and persistent embryonic eye vascularization in mice deficient in Lrp5, a Wnt coreceptor, J. Cell Biol. 157 (2002) 303–314.
[10] A. Wodarz, R. Nusse, Mechanisms of Wnt signaling in development, Annu. Rev. Cell Dev. Biol. 14 (1998) 59–88.
[11] A. Bejsovec, Wnt signaling: An embarrassment of receptors, Curr. Biol. 10 (2000) R919–R922.
[12] H. Hu, M.J. Hilton, X. Tu, K. Yu, D.M. Ornitz, F. Long, Sequential roles of Hedgehog and Wnt signaling in osteoblast development, Development 132 (2005) 49–60.
[13] Y. Kawano, R. Kypta, Secreted antagonists of the Wnt signalling pathway, J. Cell Sci. 116 (2003) 2627–2634.
[14] K. Ohnaka, H. Taniguchi, H. Kawate, H. Nawata, R. Takayanagi, Glucocorticoid enhances the expression of dickkopf-1 in human osteoblasts: Novel mechanism of glucocorticoid-induced osteoporosis, Biochem. Biophys. Res. Commun. 318 (2004) 259–264.
[15] K. Ohnaka, S. Shimoda, H. Nawata, H. Shimokawa, K. Kaibuchi, Y. Iwamoto, R. Takayanagi, Pitavastatin enhanced BMP-2 and osteocalcin expression by inhibition of Rho-associated kinase in human osteoblasts, Biochem. Biophys. Res. Commun. 287 (2001) 337–342.
[16] H. Kawate, Y. Wu, K. Ohnaka, H. Nawata, R. Takayanagi, Tob proteins suppress steroid hormone receptor-mediated transcriptional activation, Mol. Cell. Endocrinol. 230 (2005) 77–86.
[17] D.J. Chang, C. Ji, K.K. Kim, S. Casinghino, T.L. McCarthy, M. Centrella, Reduction in transforming growth factor β receptor I expression and transcription factor CBFa1 on bone cells by glucocorticoid, J. Biol. Chem. 273 (1998) 4892–4896.
[18] T. Komori, H. Yagi, S. Nomura, A. Yamaguchi, K. Sasaki, K. Deguchi, Y. Shimizu, R.T. Bronson, Y.H. Gao, M. Inada, M. Sato, R. Okamoto, Y. Kitamura, S. Yoshiki, T. Kishimoto, Targeted disruption of Cbfa1 results in a complete lack of bone formation owing to maturational arrest of osteoblasts, Cell 89 (1997) 755–764.
[19] W. Liu, S. Toyosawa, T. Furuichi, N. Kanatani, C. Yoshida, Y. Liu, M. Himeno, S. Narai, A. Yamaguchi, T. Komori, Overexpression of Cbfa1 in osteoblasts inhibits osteoblast maturation and causes osteopenia with multiple fractures, J. Cell Biol. 155 (2001) 157–166.
[20] E. Smith, G.A. Coetzee, B. Frenkel, Glucocorticoids inhibit cell cycle progression in differentiating osteoblasts via glycogen synthase kinase-3 β, J. Biol. Chem. 277 (2002) 18191–18197.
[21] H.G. Palmer, J.M. Gonzalez-Sancho, J. Espada, M.T. Berciano, I. Puig, J. Baulida, M. Quintanilla, A. Cano, A.G. de Herreros, M. Lafarga, A. Munoz, Vitamin D3 promotes the differentiation of colon carcinoma cells by the induction of E-cadherin and the inhibition of β-catenin signaling, J. Cell Biol. 154 (2001) 369–387.
[22] J.Y. Reginster, C. de Froidmont, M.P. Lecart, N. Sarlet, J.O. Defraigne, Alphacalcidol in prevention of glucocorticoid-induced osteoporosis, Calcif. Tissue Int. 65 (1999) 328–331.
[23] R.N. de Nijs, J.W. Jacobs, A. Algra, W.F. Lems, J.W. Bijlsma, Prevention and treatment of glucocorticoid-induced osteoporosis with active vitamin D3 analogues: A review with meta-analysis of randomized controlled trials including organ transplantation studies, Osteoporos. Int. 15 (2004) 589–602.

Impaired Nuclear Translocation, Nuclear Matrix Targeting, and Intranuclear Mobility of Mutant Androgen Receptors Carrying Amino Acid Substitutions in the Deoxyribonucleic Acid-Binding Domain Derived from Androgen Insensitivity Syndrome Patients

Hisaya Kawate, Yin Wu, Keizo Ohnaka, Rong-Hua Tao, Kei-ichiro Nakamura, Taijiro Okabe, Toshihiko Yanase, Hajime Nawata, and Ryoichi Takayanagi

Departments of Geriatric Medicine (H.K., Y.W., K.O., R.-H.T., R.T.) and Medicine and Bioregulatory Science (T.O., T.Y., H.N.), Graduate School of Medical Sciences, Kyushu University, Fukuoka 812-8582, Japan; and Department of the Second Anatomy (K.N.), Kurume University School of Medicine, Kurume, 830-0011, Japan

Context: Recent imaging studies revealed that androgen receptor (AR) is ligand-dependently translocated from the cytoplasm into the nucleus and forms intranuclear fine foci. In this study, we examined whether intracellular dynamics of mutant ARs detected in two androgen insensitivity syndrome (AIS) patients was impaired.

Objective: ARs with mutations in the DNA-binding domain were functionally characterized and compared with the wild-type AR.

Patients: In a complete AIS patient (subject 1), cysteine residue 579 in the first zinc finger motif of AR was substituted for phenylalanine (AR-C579F). Another mutation (AR-F582Y) was found in a partial AIS patient (subject 2).

Results: AR-F582Y retained less than 10% of the transactivation activity of the wild-type AR, whereas no ligand-dependent transactivation was detected for AR-C579F. Image analyses of the receptors fused to green fluorescent protein showed that the wild-type AR was ligand-dependently translocated into the nucleus in which it formed fine subnuclear foci. Surprisingly, after the addition of dihydrotestosterone, the two mutant ARs initially formed large cytoplasmic dots, many of which were found to be close to mitochondria by electron microscopy. Subsequently, a part of the ligand-bound mutant ARs gradually entered the nucleus to form a smaller number of larger dots, compared with the wild-type AR. Fluorescence recovery after photobleaching analysis revealed that the intranuclear mobility of the mutant ARs decreased, compared with that of the wild-type AR.

Conclusions: These results suggest that the abnormal translocation, localization, and mobility of the mutant ARs may be the cause of AIS in these subjects. (***J Clin Endocrinol Metab* 90: 6162–6169, 2005**)

ANDROGENS PLAY AN essential role in the expression of the male phenotype. The actions of androgens are mainly mediated by the androgen receptor (AR). The AR belongs to the nuclear receptor superfamily, a large group of transcription factors whose members share basic structural and functional homology (1, 2). The N-terminal domain of the AR contains the major transactivation function region, AF-1, which acts in a ligand-independent fashion. The centrally located DNA-binding domain (DBD) is highly conserved among steroid hormone receptors and consists of two zinc finger clusters. The first zinc finger motif is involved in direct DNA-binding and contains the P-box for specific recognition of the androgen-responsive elements of target genes (3). The C-terminal ligand-binding domain (LBD) contains transactivation function domain 2 and functionally interacts with intermediary factors and nuclear cofactors. In the absence of an agonist, the LBD is believed to prevent the transactivation function of the N-terminal domain through an intramolecular interaction (4).

Unliganded ARs are located in the cytoplasm, in which they are sequestered with heat shock proteins. After ligand binding, a conformational change of the receptor protein results in unmasking of both the dimerization motif and the nuclear localization signal that allows translocation into the nucleus (1). Upon nuclear entry, the ligand-receptor complexes appear to move into subnuclear compartments, which are common congregation sites for steroid hormone receptors and other associated factors, such as nuclear receptor coactivators, that are required for transcriptional activation of the target genes. Complete subnuclear foci formation seems to be essential for steroid hormone receptor-mediated transactivation (4–6).

Because the human AR gene is located on the X chromosome at Xq11–12 (1, 4, 7), just a single allele mutation in the AR gene causes dysfunction of the receptor in 46, XY individuals, resulting in androgen insensitivity syndrome (AIS) (3, 8–10). Despite a high or normal level of serum testoster-

First Published Online August 23, 2005

Abbreviations: AIS, Androgen insensitivity syndrome; AR, androgen receptor; CAIS, complete androgen insensitivity syndrome; 3D, three-dimensional; DBD, DNA-binding domain; DHT, dihydrotestosterone; FBS, fetal bovine serum; FRAP, fluorescence recovery after photobleaching; GFP, green fluorescent protein; GR, glucocorticoid receptor; LBD, ligand-binding domain; PAIS, partial androgen insensitivity syndrome; $t_{1/2}$, half-recovery time; YFP, yellow fluorescent protein.

JCEM is published monthly by The Endocrine Society (http://www.endo-society.org), the foremost professional society serving the endocrine community.

one, AIS patients show various phenotypic abnormalities of male sexual development. AIS is subdivided into three phenotypes: complete androgen insensitivity syndrome (CAIS), partial androgen insensitivity syndrome (PAIS), and mild androgen insensitivity syndrome. AR mutations that severely impair the function of the AR cause CAIS. The main phenotypic characteristics of individuals with CAIS are female external genitalia with a short, blind-ending vagina, absent Müllerian duct, and absence of pubic and axillary hair. The gender identity is that of a normal female, but testes are commonly located in either the abdomen or the inguinal area and the uterus is absent. Laboratory findings show the 46, XY karyotype, normal or increased synthesis of testosterone by the testes, and a normal or increased level of LH. PAIS patients also show female-like external genitalia, except for clitoromegaly and/or posterior labial fusion (3, 9). Although mutations responsible for AIS are spread throughout the AR gene, there are hot spots, especially at exon 5, which encodes part of the LBD (Androgen Receptor Gene Mutation Database: www.mcgill.ca/androgendb).

We previously reported two unrelated AIS patients (one CAIS and one PAIS) carrying amino acid substitutions in the first zinc finger motif of the AR-DBD (11). In the CAIS patient (subject 1), cysteine residue 579, which coordinates a zinc ion, was substituted with phenylalanine, and the mutant AR showed almost no ligand-induced transcriptional activation. On the other hand, the AR-F582Y mutant found in the PAIS patient (subject 2) showed much less transactivation than the wild-type AR. Here, to visualize any dynamic changes of the intracellular localizations of these mutant ARs, the wild-type and mutant ARs were fused with green fluorescent protein (GFP) and their intracellular movements were analyzed using a laser confocal microscope. After treatment with the ligand, the wild-type AR was translocated from the cytoplasm into the nucleus in which it formed fine subnuclear foci. In contrast, the AR-DBD mutants initially formed large cytoplasmic dots, many of which were located close to mitochondria after the addition of dihydrotestosterone (DHT), and a proportion of the proteins subsequently moved into the nucleus to become located in subnuclear bodies. The subnuclear foci of the mutant ARs were characterized by their larger size, much smaller number, and lower mobility, compared with the wild-type AR. These results indicate that the pathogenesis of AIS in these two patients may be caused by the mislocation and lower mobility of their mutant ARs.

Subjects and Methods

Subjects

Subjects 1 and 2 were diagnosed with CAIS and PAIS, respectively, and had missense mutations of Cys^{579} to Phe and Phe^{582} to Tyr, respectively. The clinical history and data of the AIS patients characterized in the present study were previously reported (11).

Cells

COS-7 monkey kidney cells were obtained from the Riken Cell Bank (Tokyo, Japan) and maintained in DMEM (Invitrogen, Carlsbad, CA) containing antibiotics and 10% fetal bovine serum (FBS; Cansera International Inc., Etobicoke, Canada).

Plasmids

The firefly luciferase reporter plasmids, pGL3-MMTV (5) and pGL3-PSA (12), and the expression vectors for AR (pCMV-AR) were prepared as previously described (13, 14). The plasmid vectors pAR-GFP (5) and pAR-CFP (6) for expression of the AR-GFP and AR-CFP fusion proteins were constructed as described previously. Expression plasmids of the mutant ARs for mammalian cells, designated pCMV-AR-C579F (from subject 1) and pCMV-AR-F582Y (from subject 2), were constructed as previously reported (11). To construct a GFP fusion protein of the mutant AR for subject 1, a *KpnI-ScaI* fragment of pCMV-AR-C579F, which contained the mutated site, was replaced with that of pAR-GFP to generate pAR-C579F-GFP. Similarly, for subject 2, a *HindIII-ScaI* fragment of pAR-GFP was replaced with that of pCMV-AR-F582Y to construct pAR-F582Y-GFP. The validity of the structure of each construct was confirmed by DNA sequencing using an ABI PRISM 377 DNA sequencer (Applied Biosystems, Foster City, CA).

Immunoblotting

COS-7 cells were seeded in 100-mm plates and incubated for 24 h in 5% CO_2 at 37 C. Five micrograms of plasmid DNA carrying the wild-type or a mutant AR was transfected into the cells using 20 μl Superfect transfection reagent (QIAGEN GmbH, Hilden, Germany). Twenty-four hours after the transfection, the cells were washed twice with PBS and then 400 μl of Nonidet P-40 lysis buffer [50 mM Tris-HCl (pH 8.0), 150 mM NaCl, and 1% Nonidet P-40] was added to each dish, followed by rocking for 30 min at 4 C. Lysates were collected by centrifugation and the protein concentrations were measured using a BCA protein assay kit (Pierce, Rockford IL). Next, 40 μg of each lysate in 1× SDS-PAGE sample buffer [2% sodium dodecyl sulfate, 100 mM dithiothreitol, 60 mM Tris-HCl (pH 6.8), and 0.01% bromophenol blue] was loaded onto a sodium dodecyl sulfate-polyacrylamide gel (10% separating gel) and electrophoresed at 20 mA for 4 h. Proteins were transferred onto nitrocellulose membrane (Hybond P; Amersham Biosciences, Piscataway, NJ) using a Trans-Blot SD Semi-Dry transfer cell (Bio-Rad Laboratories, Hercules, CA) at 250 V for 1 h at 25 C. After blocking the membrane in 1× Block-Ace (Dainippon Pharmaceutical Co., Osaka, Japan), an anti-AR polyclonal antibody (sc-816; Santa Cruz Biotechnology Inc., Santa Cruz, CA) was reacted with the membrane in 0.1× Block-Ace for 1 h at 25 C. After a brief wash with Tris-buffered saline-Tween 20 (10 mM Tris-HCl, 0.9% NaCl, and 0.05% Tween 20), horseradish peroxidase-conjugated antirabbit Ig antibodies (Amersham Biosciences) were added in 0.1× Block-Ace as the secondary antibody, and the membrane was incubated for 45 min at 25 C with gentle shaking. After washing with Tris-buffered saline-Tween 20, the membrane was reacted with Western blotting detection reagents (Amersham Biosciences) for 1 min in a dark room. The labeled protein bands were visualized and analyzed using a VersaDoc imaging system 5000 (Bio-Rad).

Functional reporter assays

COS-7 cells (1 $\times 10^5$ cells/well) were seeded in 12-well plates at 20 h before transfection. Cells were cotransfected with 0.5 μg/well of pGL3-MMTV as a reporter plasmid, 2 ng/well of pRL-CMV (Promega Corp., Madison, WI) as an internal control, and 0.1 μg/well of a wild-type or mutant AR expression plasmid with 1.7 μl/well of Superfect. In all transfection experiments, the total amount of plasmid DNA was fixed by adding empty vector to the transfection mixture. At 3 h after transfection, 0.5 ml of DMEM containing 10% charcoal-treated FBS was added with or without steroid hormone (10^{-8} M DHT). After incubation for 24 h, the cells were rinsed with PBS and lysed in the lysis buffer contained in a luciferase assay kit (Promega). The luciferase activity was assayed using the dual-luciferase assay system (Promega) and a Lumat LB 9507 (Berthold Technologies, Bad Wildbad, Germany). Each value was determined as the average of three independent experiments. Data were presented as the means ± SD. One-way ANOVA followed by Scheffé's test was used for multigroup comparisons. $P < 0.05$ was considered to be statistically significant

Confocal laser-scanning microscopy

For living cell microscopy, COS-7 cells (2 $\times 10^5$ cells/well) were seeded in 35-mm glass-bottom dishes (Asahi Techno Glass Corp., Tokyo,

Japan) and transfected with 0.5 μg of plasmid DNA carrying the wild-type or a mutant AR fused with GFP or yellow fluorescent protein (YFP) using 5 μl/well Superfect. The cells were maintained in DMEM supplemented with 10% charcoal-treated FBS for 20 h, and then various steroid hormones were added to the medium. The cells were observed with an Axiovert 200M inverted microscope equipped with an LSM510META scan head (Carl Zeiss, Jena, Germany) using a ×100, 1.4 numerical aperture oil immersion objective. Images were collected at a 12-bit depth resolution of intensities over 1024 × 1024 pixels. For excitation of GFP and YFP, a 488-nm argon laser was used and a series of images was obtained. The GFP and YFP signals were separated using the emission fingerprinting technique established by Carl Zeiss. Separation of the individual emission signals was based on recording a spectral signature and applying a linear unmixing algorithm using the reference spectra of each fluorescent protein (15).

To construct three-dimensional (3D) images, a series of 30–50 two-dimensional tomographic images were collected for each cell using the confocal microscope. These images were exported as TIF files and the TRI graphic program (Ratoc System Engineering, Tokyo, Japan) was used to reconstruct 3D images (6). Both the spatial distribution and calculation of the fluorescent proteins as distinct volumes were made possible by removing scattering background fluorescence and lens spherical aberrations and then separating each particle (6). The numbers of subnuclear foci determined for the wild-type and mutant ARs were representative of at least 20 cells.

Fluorescence recovery after photobleaching (FRAP) analysis

Cells were transfected with the wild-type AR and a mutant AR and incubated for 24 h at 37 C. After a further 5-h incubation with DHT, FRAP analysis was performed. After collection of the initial image using a Carl Zeiss LSM510META microscope, a selected area of a fixed size in the nucleus was photobleached by setting the laser wavelength to 488 nm and using the maximum power for 50 iterations. After the bleaching, images within the bleached region were taken every second at a resolution of 512 × 512 pixels to follow the recovery of the fluorescence intensity. The intensity of the fluorescence was calculated using the LSM510 software and the half-recovery time ($t_{1/2}$) was determined as the time when the fluorescence intensity reached half the maximal recovery using the Microsoft Excel software. Each $t_{1/2}$ was the average of six to 10 FRAP experiments.

Organelle detection

COS-7 cells were transfected with pAR-C579F-GFP. Twenty-four hours after the transfection, the cells were treated with DHT and then LysoTracker Red or MitoTracker Orange CMTMRos (Molecular Probes Inc., Eugene, OR) was added in the medium at a final concentration of 100 nM to visualize the lysosomes or mitochondria, respectively. The cells were incubated for 30 min at 37 C and then rinsed with PBS. Images were collected using the fluorescence microscope.

Immunoelectron microscopy

Twenty-four hours before transfection, COS-7 cells were seeded in a 60-mm dish. The cells were transfected with 2 μg of pAR-C579F-GFP using 3 μl of Superfect. After incubation for 20 h, the cells were treated with 10^{-8} M DHT for 1 h. After a brief wash with PBS, the cells were fixed in 0.1% glutaraldehyde in 0.1 M phosphate buffer (pH 7.4) for 30 min at 25 C. The fixed cells were scraped off the dish, centrifuged at 5000 × *g* for 10 min at 4 C and resuspended in 0.1 M phosphate buffer. After dehydration in a graded series of ethanol, the cell pellet was embedded in LR White resin and ultrathin sections were cut (16). After blocking in 0.1 M phosphate buffer containing 3% BSA, the sections were incubated with rabbit polyclonal antibodies against GFP (BD Biosciences Clontech, Mountain View, CA) at 1:1000 dilution in 0.1 M phosphate buffer at 4 C overnight, followed by incubation with colloidal gold (Ø = 15 nm)-conjugated goat antirabbit IgG (Amersham Biosciences) at 1:100 dilution. After washing with distilled water, the sections was stained with 2% uranyl acetate and lead citrate, and observed with a Hitachi H-7000 electron microscope (Hitachinaka, Japan).

Results

Previously we found two different amino acid substitutions in the DBD of ARs derived from AIS patients (11). One mutation from a CAIS patient (subject 1) occurred at Cys579 which coordinates a zinc ion in the first zinc finger motif of the AR (Fig. 1A). This residue also forms a P-box that is important for the recognition of an androgen-responsive element in target genes. The other mutation from a PAIS patient (subject 2) was found at Phe582 next to the P-box (Fig. 1A). To compare the functions of these two mutant ARs with the wild-type AR, recombinant AR proteins were expressed in COS-7 cells. Immunoblot analysis showed that the expression levels of the wild-type and mutant ARs in transfected cells were almost the same (Fig. 1B). To examine AR-mediated transcriptional activation, luciferase assays were performed using the MMTV promoter containing several hormone-responsive elements (17). For the wild-type AR,

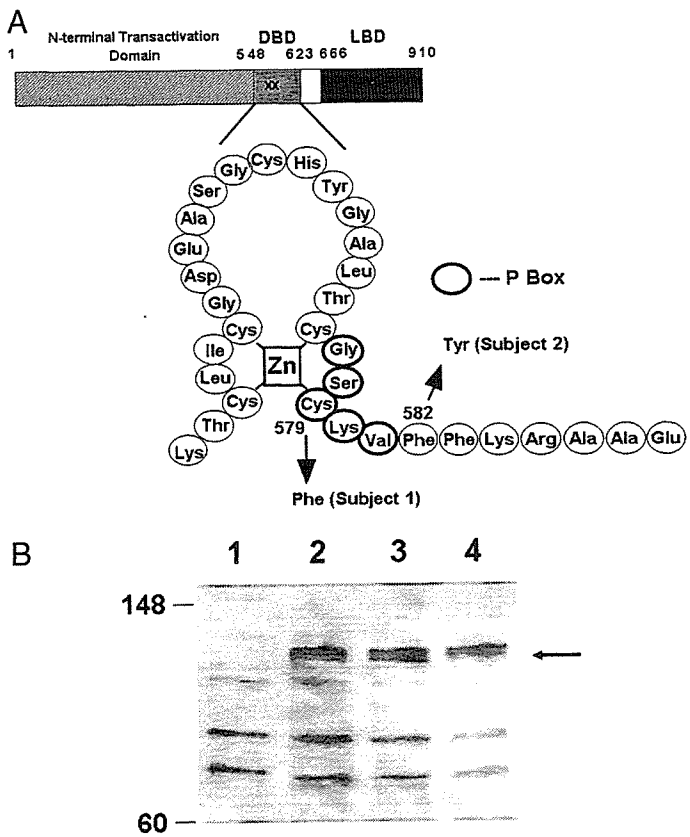

FIG. 1. The amino acid substitutions in the two AIS patients are located in the DBD of the AR. A, Schematic representation of the AR and the sites of the amino acid substitutions detected in the AIS patients. The *upper scheme* shows the domain structure of the AR: the N-terminal domain, the DBD, and the C-terminal LBD. Two different amino acid substitutions (x) were identified in the DBD of the ARs from these two AIS patients. The first zinc finger motif of the AR-DBD is magnified in the *lower scheme*. The five amino acids *circled in bold* indicate the P-box. The *arrows* indicate the amino acid substitutions in the two AIS patients. In subject 1, the cysteine at position 579 involved in the P-box is substituted by phenylalanine (C579F). In subject 2, phenylalanine 582 is changed for tyrosine (F582Y). B, Immunoblot analysis of wild-type and mutant ARs in COS-7 cells. Cells were transfected with a wild-type or mutant AR expression vector using Superfect. Twenty-four hours after the transfection, the cells were lysed and subjected to immunoblotting analysis as described in *Subjects and Methods*. Anti-AR antibodies were used for detection. The *arrow* shows the AR bands. Lane 1, Vector only; lane 2, wild-type AR; lane 3, AR-F582Y; lane 4, AR-C579F. The *numbers on the left* of the gel show the positions of protein size markers.

remarkable transcriptional activation was observed after addition of the ligand DHT. On the other hand, AR-F582Y showed less than 10% of the transcriptional activation of the wild-type AR, whereas AR-C579F showed no ligand-dependent transactivation at all (Fig. 2).

To visualize the subcellular localizations of the wild-type and mutant ARs, GFP-fusion proteins were generated and observed under a confocal laser-scanning microscope. As we previously reported, the wild-type AR was diffusely localized in the cytoplasm in the absence of the ligand (Fig. 3A) (5). Upon treatment with the ligand, the wild-type AR was almost completely translocated from the cytoplasm into the nucleus in which it formed subnuclear fine foci (Fig. 3D). The AR-DBD mutants were also diffusely present in the cytoplasm before addition of the ligand (Fig. 3, B and C). However, in contrast to the wild-type AR, the two mutant ARs formed cytoplasmic dots after the addition of DHT (Fig. 3, E and F). Time-course experiments revealed that most of the fluorescent signals for the wild-type AR were observed in the nucleus within 30 min after the addition of DHT (Fig. 4B), whereas cells expressing the AR-C579F mutant showed two patterns (Fig. 4, E–H or I–L). Approximately 80% of cells formed the cytoplasmic dots and a limited number of nuclear foci 30 min after the addition of DHT (Fig. 4F), and the nuclear dots became clear at 3 h after the ligand addition (Fig. 4H). In the other type of AR-C579F-expressing cells (20%), cytoplasmic dots were not so striking (Fig. 4J), but delayed nuclear translocation with dot formation of mutant AR was observed (Fig. 4L). In both types of the mutant-expressing cells, a smaller number of larger-sized intranuclear dots for

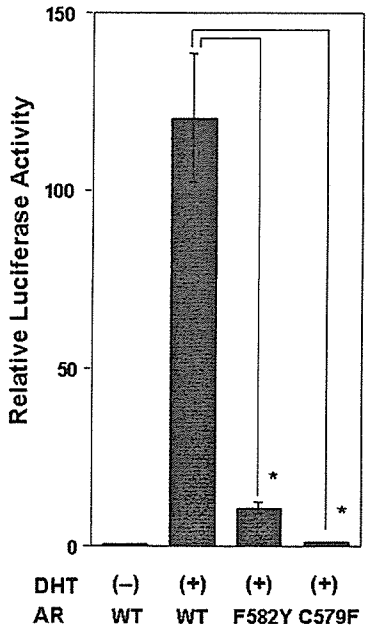

FIG. 2. Effects of the two different amino acid substitutions in the AR-DBD on transcriptional activation. COS-7 cells were transiently transfected with plasmid DNA expressing the wild-type (WT) or a mutant (C579F or F582Y) AR, pGL3-MMTV as a reporter plasmid, and pRL-CMV as an internal control. After treatment with or without 10^{-8} M DHT for 24 h, the luciferase activity was measured. The *bars* show the luciferase activities of the transfected cells relative to the value of the wild-type AR without DHT. The means ± SD of three independent experiments are shown. *, $P < 0.05$.

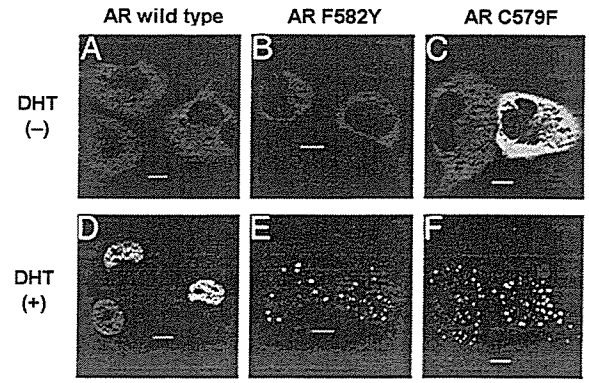

FIG. 3. Ligand-dependent translocation of the wild-type and mutant ARs. COS-7 cells were transfected with 0.5 μg of each plasmid DNA expressing GFP-fused wild-type AR (A and D), AR-F582Y (B and E), or AR-C579F (C and F). Fluorescent signals were observed at 24 h after the transfection under a laser confocal microscope (A–C). Subsequently 10^{-8} M DHT was added and incubated at 37 C for 1 h and the ligand-bound receptor proteins were observed (D–F). *Scale bar*, 10 μm.

AR-C579F were observed, compared with those for the wild-type AR (Fig. 4, D, H, and L). Even after a 3-h treatment with the ligand, a significant amount of the mutant AR still remained in the cytoplasm (Fig. 4, H and L), whereas almost all the signals for the wild-type AR were detected in the nucleus (Fig. 4D). These data indicate that the nuclear translocation and subnuclear localization are impaired in AR-DBD mutants.

To quantitatively analyze the subnuclear foci, 3D images were constructed from the tomographic images collected using the confocal microscope. As shown in Fig. 5, both the C579F and F582Y AR mutants had a much lower number of foci in the nucleus than the wild-type AR. The average number of nuclear foci for the wild-type AR was 300 ± 8, whereas the numbers for F582Y and C579F were 106 ± 18 and 127 ± 23, respectively.

To examine whether the mutant ARs inhibit the nuclear translocation of the wild-type AR, we cotransfected the wild-type AR fused to GFP (AR-WT-GFP) and AR-C579F-CMV (without GFP) and observed the cells under the confocal microscope. Cotransfection of AR-WT-GFP with AR-C579F-CMV showed cytoplasmic dots in addition to fine nuclear foci after treatment with DHT (Fig. 6Ab). Opposite experiments using AR-C579F-GFP and AR-WT-CMV led to similar results, revealing that both nuclear and cytoplasmic dots appeared after incubation with DHT (Fig. 6Ad). To confirm the colocalization of the wild-type and mutant ARs, AR-WT-CFP and AR-C579F-GFP were coexpressed, and each fluorescent signal was collected under the laser confocal microscope. As shown in Fig. 6B, wild-type and mutant ARs were colocalized in both the nuclear and cytoplasmic dots in the presence of 10 nM DHT (Fig. 6B, d–f). The magnitude of the transcriptional activation in the cells transfected with both AR-WT and AR-C579F was less than half that induced by AR-WT (Fig. 6C). In addition to this experiment using 10 nM DHT, we measured the transcriptional activation of the wild-type AR in the presence of 5 nM DHT. The reporter luciferase activity of the wild-type at 5 nM DHT was significantly higher than that by combination of the wild-type and

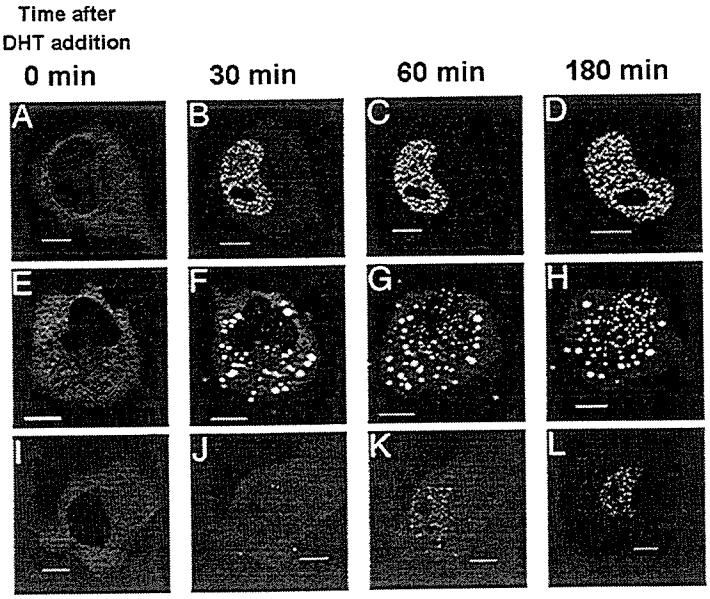

FIG. 4. Time-lapse translocation of wild-type (WT) and mutant ARs after the addition of DHT. COS-7 cells expressing wild-type AR (A–D) or the AR-C579F mutant (E–H and I–L) were treated with 10^{-8} M DHT. Images were collected using a laser confocal microscope before the DHT treatment (A, E, and I) and at 30 (B, F, and J), 60 (C, G, and K), and 180 min (D, H, and L) after the treatment. *Scale bar*, 10 μm.

AR-C579F at 10 nM. Even in a high dose of DHT (100 nM), which can fill all the wild-type LBD, coexpression of AR-C579F inhibited the transcriptional activation mediated by the wild-type AR (Fig. 6C). These results indicated that simple stealing of ligand by AR-C579F is not able to explain the suppression effect of AR-C579F and strongly suggested that AR-C579F is able to form heterodimers with AR-WT in the cells and inhibit the translocation of AR-WT, thereby reducing the transactivation.

As shown in Figs. 4 and 5, the numbers of nuclear foci for the mutant ARs were much lower than that for the wild-type AR. To evaluate whether there are any differences in dynamics between the nuclear foci of the wild-type and mutant ARs, the mobilities of the wild-type and mutant ARs in the nucleus were measured quantitatively by FRAP analysis. After a short period of photobleaching at the maximal power of the laser, continuous images were taken at 1-sec intervals. As shown in Fig. 7A, the recovery of the fluorescence intensity for AR-C579F foci was slower than that for AR-WT. The fluorescence recovery was evaluated by plotting the intensity of the bleached area against time (Fig. 7B). Compared with the wild-type AR, the slope of the fluorescence recovery of AR-C579F was relatively gentle. The $t_{1/2}$ for AR-C579F was 10.5 ± 1.6 sec (n = 12), which was significantly slower than

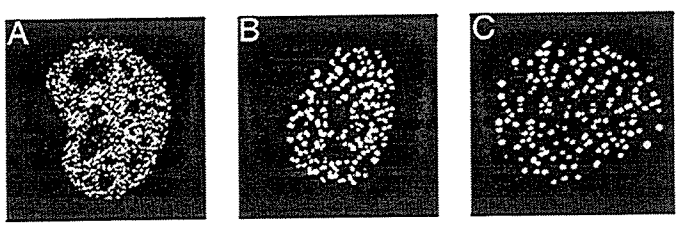

FIG. 5. Three-dimensional image analyses of the intranuclear foci of the wild-type and mutant ARs. COS-7 cells were transfected with 0.5 μg of pAR-GFP (A), pAR-F582Y-GFP (B), or pAR-C579F-GFP (C). Twenty-four hours after the transfection, the cells were treated with DHT and two-dimensional tomographic images collected using the confocal microscope were used to reconstruct 3D images as described in *Subjects and Methods*.

that for the wild-type AR [8.0 ± 1.1 sec (n = 10)]. In another experiment, AR-F582Y also showed reduced mobility, compared with the wild type [$t_{1/2}$ = 8.4 ± 1.1 sec (n = 6)], and the $t_{1/2}$ for AR-F582Y [9.9 ± 1.2 sec (n = 6)] was almost the same as that for AR-C579F [10.2 ± 1.1 sec (n = 6)]. These results indicate that the DBD amino acid substitution in the mutant AR caused decreased mobility of the AR in the nucleus.

As shown in Fig. 3, AR-DBD mutants showed ligand-dependent formation of large cytoplasmic dots. We investigated the localizations of the mutant ARs in the cytoplasm after the ligand treatment. The mutant ARs were not localized in the lysosomes, as shown by an experiment using LysoTracker, a specific marker for lysosomes (data not shown). Next, the mitochondrial localization was examined using MitoTracker, a highly specific probe for mitochondria. Many, but not all, of the cytoplasmic dots of the mutant ARs were located close to mitochondria (Fig. 8A). Because signals for the mutant ARs were not observed in the mitochondria, the mutant ARs do not seem to cross the mitochondrial membrane. To further examine the relationship between the mutant ARs and the mitochondria, immunoelectron microscopy was performed using an anti-GFP antibody. Many gold labels were present around the mitochondria, but none were found inside the mitochondria (Fig. 8Ba). Some clusters were present in the cytoplasm, and these would correspond to the cytoplasmic dots observed by the laser-scanning microscopy (Fig. 8Bb).

Discussion

Using fluorescent proteins and laser-scanning microscopy, we have demonstrated that mutations in the DBD of ARs from AIS patients impair the ligand-dependent nuclear translocation, subnuclear foci formation, and intranuclear mobility of the receptor. In our previous studies, we clearly showed that intranuclear foci formation of AR-GFP was parallel to ligand-dependent transcriptional activation of AR (5, 6). Many studies using GFP-fused steroid hormone receptors have been reported, and linkage of the foci formation of